Wireless Charging System

for the Wireless Powerlizer

B. P. M. Hurkmans
F. H. van der Kolk

Bachelor Thesis

July 9, 2021

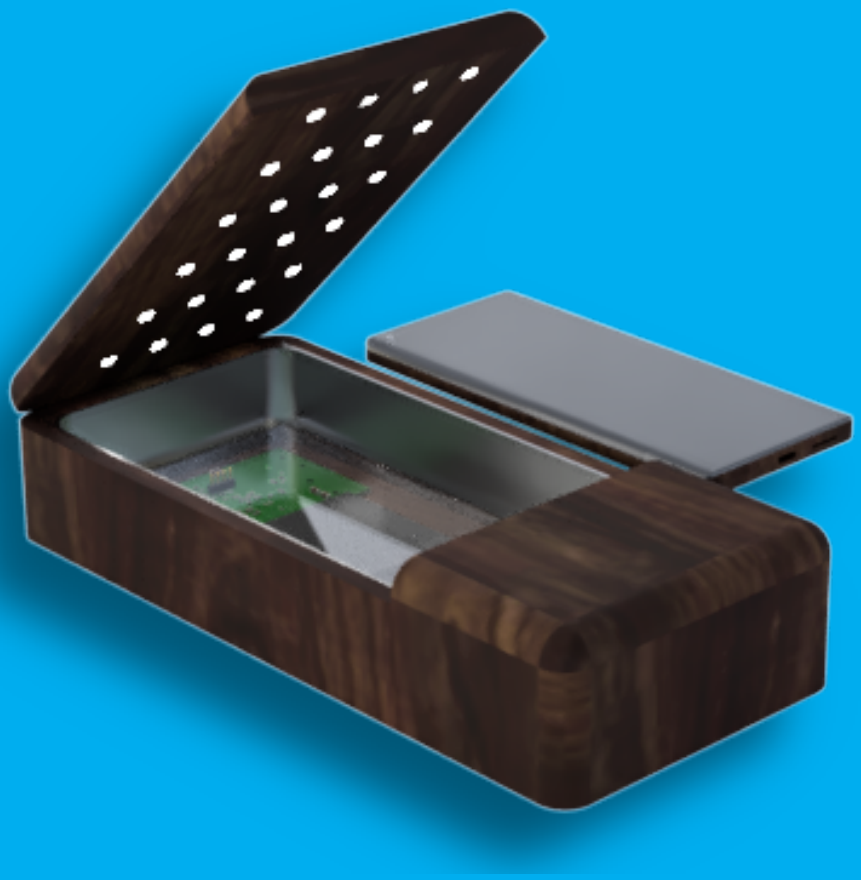

TU Delft

Wireless Charging System

for the Wireless Powerlizer

by

B. P. M. Hurkmans
F. H. van der Kolk

to obtain the degree of Bachelor of Science
at the Delft University of Technology.

Authors:	B. P. M. Hurkmans	4952391
	F. H. van der Kolk	4961404
Project duration:	April 19, 2021 – July 2, 2021	
Supervisors:	Dr. J. Dong,	
	W. Shi.	
Thesis committee:	Dr. ing. I. E. Lager,	TU Delft
	Dr. J. Dong,	TU Delft
	Dr. T. B. Soeiro.	TU Delft

An electronic version of this thesis is available at http://repository.tudelft.nl/.

TU Delft

Abstract

Wireless power transfer has been around for a long time. In 1899 Nikola Tesla demonstrated that it was possible to transfer power using a pair of coils. This technology has advanced to now charge a wide range of portable devices, such as phones. In this thesis, a wireless charging system is designed to be integrated into a power bank with UV-C sterilization to charge phones.

The design focuses on creating a small and highly efficient module to transfer energy from the power bank battery to the phone with as little losses as possible. The design adheres to the Qi standard from the Wireless Power Consortium by following the MP-A2 reference design. The design consists of a voltage regulator to provide a constant voltage, a controlled inverter that manages output power, and a series compensated transmitter coil. LTspice simulations predict the power efficiency to be 74 % from the battery to the receiver. A prototype PCB was designed and assembled to demonstrate the performance of the design in practice and transferred 5 W at an efficiency of 67 %. This shows potential for future integration of the design into the power bank.

Preface

This thesis was written in the context of the EE3L11 Bachelor Graduation Project for the Electrical Engineering program.

In this project the objective was to design the Wireless Powerlizer: a combination of a power bank that allows for wireless charging, and a UV-C sterilizer. This project was divided into three different subgroups, and our focus will be on the wireless charging unit.

We want to thank our supervisors: Dr. Jianning Dong, Wenli Shi, and Dr. Tiago Batista Soeiro for their support and assistance during this project and for making this project possible. We also want to extend our gratitude to Calvin Riekerk and Guangyao Yu, the daily supervisors of the other subgroups, and Bart Roodenburg and Harrie Olsthoorn, the technicians of the DCE&S Group who helped us with assembling our PCB. Finally, a loving thanks to our group members: Jeroen Ammers, Hsukang Chen, Charlotte De Jonghe and Gijs Lagerweij.

Brecht Hurkmans
Floris van der Kolk
Delft, June 2021

Contents

1 Introduction

Due to the current COVID-19 pandemic, there has been a focus on hygiene and disinfection. Liquid disinfection is often used to disinfect surfaces. Another way to solve this problem, is using UV-C light to eliminate microbes on surfaces like mobile phones. By integrating a UV-C disinfection system into a portable power bank, it is possible to disinfect objects anywhere. During the disinfection process, the mobile device can also be conveniently charged by making use of wireless charging technology. This thesis will outline the design process of a wireless charging system that can be used in this application.

1.1. Project Objective

The aim of this project is to develop a power bank that can charge a mobile phone wirelessly and sterilize personal belongings such as keys, mobile phones, or face masks using UV-C light. The final product will be a portable box called the Wireless Powerlizer which integrates a power bank and its management circuit, a wireless charging coil and its control circuit, and a UV-C generator for sterilization. The system-level architecture is presented in Figure 1.1. The subsystem highlighted in green will be discussed in this thesis, as well as a conceptual design of (a part of) the high-level controller. The yellow battery management system and the UV-C sterilizer are designed by different teams [1, 2].

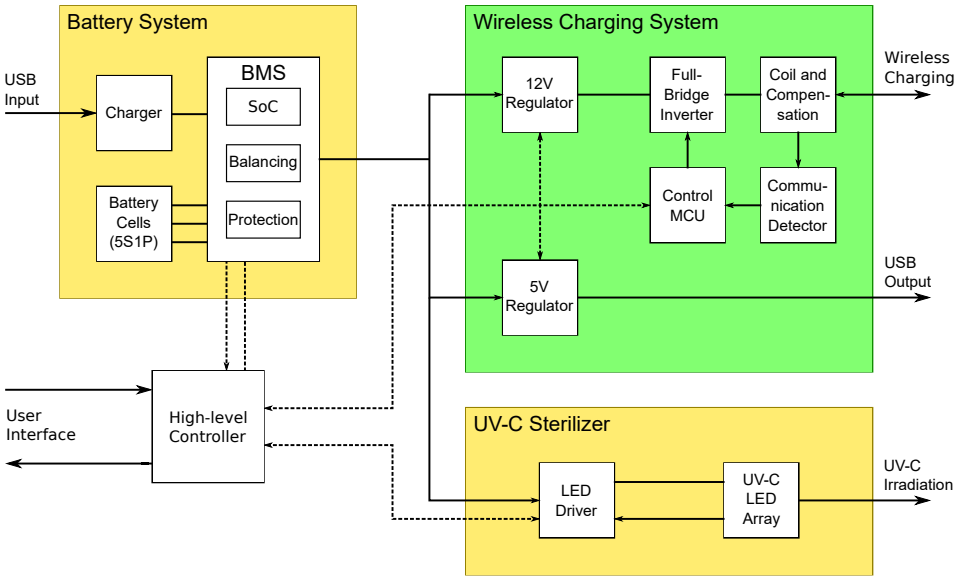

Figure 1.1: System-level architecture block diagram of the Powerlizer.

1.2. Analysis

Wireless power transfer has been around for a long time. In 1899 Nikola Tesla demonstrated that it was possible to transfer power wirelessly using coils. Since that time, research has been conducted to create smaller and more efficient systems. This was made possible by the use of transistors and further advancements in power electronics.

Wireless power transfer can be accomplished in many ways. A popular method is resonant magnetic power transfer for short ranges. Here, a coil is used to transfer power using a magnetic field to form a link to another coil through the air. These coils are compensated in some way to achieve a higher efficiency [3–6]. Since this coil radiates magnetic fields, it should comply to the relevant regulations.

Due to the magnetic resonant link in wireless charging, a lot of energy is lost. To get a feeling for the efficiency of wireless charging, a 5 W USB Qi wireless charging pad [7] and receiver [8] were tested on their efficiency. This came out to be 46 %.

Resonant magnetic power transfer is incorporated in many mobile devices, like mobile phones. In 2010, the Wireless Power Consortium started publishing the Qi standard, which is often used for these devices to ensure compatibility. The Qi standard includes multiple power profiles, for 5 W and 15 W power transfer. It also features requirements for its operating surface temperature, as well as its ability to not transfer power to non-wireless charging capable objects.

1.3. Thesis Outline

An outline of the requirements of the system will be given in Chapter 2. The basis of wireless charging will be described in Chapter 3. The design of the wireless charging system of the Wireless Powerlizer will be discussed in Chapters 5 and 6. After that, the prototype will be discussed in Chapter 7 and at the end the conclusions will be presented in Chapter 8.

2

Program of Requirements

In this chapter, the requirements for the top-level system as well as the wireless charging system will be discussed.

2.1. Powerlizer Requirements

The requirements for the entire Wireless Powerlizer system are derived from the project objective, and can be divided into several categories. The functional requirements specify what functionality the system must provide.

[**SF.1**] The Powerlizer shall be able to provide two full (0–100 %) wireless phone charges to a phone with average battery capacity (roughly 3500 mA h). This will determine the minimum required battery capacity, as well as the wireless charging time.

[**SF.2**] The Powerlizer shall have a USB-C port for charging the internal battery. An official USB protocol shall be supported.

[**SF.3**] The Powerlizer shall be able to disinfect an area of 10 cm × 17.5 cm. These dimensions are chosen such that most modern smartphones will fit in the disinfection area. Modern smartphone dimensions typically range between 65–80 mm width, 145–170 mm height, and 7.5–10 mm thickness.

- [**SF.3.1**] The disinfection should inactivate the most common microbes found on mobile phones.
- [**SF.3.2**] The disinfection should inactivate at least 99 % and preferably even 99.9 % of these microbes. This corresponds to a 2 or 3 log reduction, respectively.

[**SF.4**] The state of charge of the power bank shall be displayed on an LED indicator. These LEDs may also be used for other user interface purposes (such as displaying disinfection status, wireless charging status, etc.)

Taking into account the portable nature of the Wireless Powerlizer, the allowable operating conditions, aspects of the enclosure, and product dimensions must be considered.

[**SO.1**] The Powerlizer shall be able to operate in a temperature range between 0–45 °C. The allowable temperature range is limited by the battery cells.

[**SO.2**] The Powerlizer enclosure shall be

- [**SO.2.1**] Capable of withstanding temperatures up to 60 °C.
- [**SO.2.2**] Splash resistant.

[**SO.3**] The Powerlizer enclosure shall be at most 12.5 cm × 27.5 cm × 6 cm.

Safety is another important aspect since the Powerlizer will be used in close proximity to humans.

[**SS.1**] The Powerlizer shall follow the relevant IEC, ISO, and national safety regulations.

[**SS.2**] The disinfection area shall not be accessible while the disinfection LEDs are turned on. If the area is opened, disinfection must stop as soon as possible.

[**SS.3**] The wireless charging system must comply with EMI, electromagnetic field exposure, and safety regulations.

2.2. Wireless Charging System Requirements

Mandatory:

[**M.1**] The wireless charging system should conform to the Qi standard [9].

[**M.2**] The system should be capable of delivering 15 W to a Qi-capable power receiver.

[**M.3**] The wireless charging system should have a minimum efficiency of 50 % at 15 W.

[**M.4**] The input voltage range is determined by the battery to be 15 to 21 V (fully charged/discharged) [1].

[**M.5**] The system should have Foreign Object Detection (FOD) to detect objects that are not capable of being charged and avoid transferring power to them.

[**M.6**] The coils should fit in an area of 10 cm $\times$ 17.5 cm, set by the Sterilizer system [2].

[**M.7**] The interface surface should stay below 12 K above ambient temperature while operating for 1 hour (under normal operating conditions).

Safety requirements to be met:

[**S.1**] The final commericial product should conform to the IEC 63245-1:2021 related to wireless power transfer and CISPR 14-1:2020 related to EMC regulations.

Specifications that require a Trade-off:

[**T.1**] If possible, a 5 V USB type A output for wired charging could be added.

[**T.2**] The switching frequency of the voltage regulator should be >200 kHz to not influence the wireless communication.

3

Wireless Power Transfer

An alternative to wired charging of mobile devices is wireless charging. There are several ways to accomplish wireless power transfer to realize . These methods will be discussed in this chapter. Also, an in-depth explanation of the chosen method will be given.

3.1. Wireless Power Transfer Methods

To transfer power wirelessly from a transmitter to a receiver, lasers can be used [10]. In this way, electromagnetic waves in the form of light can be focused on a small point. These waves can then be received and converted into electrical power. The main disadvantage is that a line of sight needs to be maintained between the transmitter and receiver. This means that there can't be any obstructions between them.

Capacitive power transfer is also possible [11]. Here, two parallel plates are coupled using an electric field. This type of transfer requires a high voltage, large surface area, a high frequency, and a small distance to work [12].

For inductive power transfer, two coils are coupled using a magnetic field. Resonant magnetic power transfer is very similar to inductive power transfer. The main difference is that compensation is added to operate efficiently below the self-resonant frequency of the coils [13]. Another advantage is that a flat coil can be used to integrate into a compact design.

All methods of wireless power transfer have several advantages and disadvantages. Modern mobile devices have mostly moved to resonant magnetic power transfer. This is most likely due to its relative safety and efficiency [14, 15].

3.2. Magnetic Resonance WPT

Wireless power transfer is used in transformers. The difference between wireless chargers and transformers is the coupling coefficient (k). Transformers have a laminated steel core that is physically connected between the primary- and secondary coil. The values for k can approach a value of almost 1. For wireless chargers, the cores often consists of air and so the coils are more loosely coupled. A current through the primary coil of the transformer excites a magnetic field, according to Ampère's Law (Equation 3.1).

$$\oint \vec{B} \cdot d\vec{l} = \mu I \tag{3.1}$$

This magnetic field has a flux through the surface area (A) of the receiving coil as described in Equation 3.2.

$$\phi = \iint_A \vec{B} \cdot d\vec{A} \tag{3.2}$$

If this flux changes in time, a voltage is induced in the secondary coil of the transformer. This is described in Equation 3.3.

$$\oint \vec{E} \cdot d\vec{l} = -\frac{d\phi}{dt} \tag{3.3}$$

This means that by driving a primary coil with a changing current, a voltage can be excited in the secondary coil, and thus power transfer is achieved.

3.2.1. Compensation

The coils used for the power transfer can be compensated for efficient power transfer around a certain resonant frequency. The reactive power should be minimized to compensate a coil and maximize the efficiency. This can be done in several ways. A capacitor can be added in series with the transmitting and receiving coil or in series with the transmitting coil and in parallel with the receiving coil [4]. Also, inductors can be added in series. This can be seen in [5]. It is even possible to only compensate the primary side [6]. Several methods of compensation are compared in [3]. Different output characteristics can be achieved depending on the topology.

In the Qi standard reference designs, series compensation is used on the primary side. On the secondary side, capacitors are added both in series and in parallel. In this way, small capacitors are used instead of bigger inductors. There are also a small number of components while still providing a constant voltage output [16].

3.2.2. Full-bridge Inverter

An inverter is used to drive the coil with an alternating current (AC) from a direct current (DC) source. AC is needed to create an alternating magnetic field which in turn creates an alternating flux through the secondary coil for an electromotive force. An inverter can be implemented using a full-bridge inverter [17]. The topology can be seen in Figure 3.1. By providing a high signal to s1 and s4, the current will flow as indicated by I_L. In this case, a low signal has to be provided to s2 and s3 to not short-circuit the supply. By providing a high signal to s2 and s3 (s1 and s4 low), a current in the opposite direction can be created. A combination of these two steps can be used to create an alternating current through the coil. The body diodes will conduct the current from the collapsing magnetic field in the coil during the time that the transistors are turned off (dead-time).

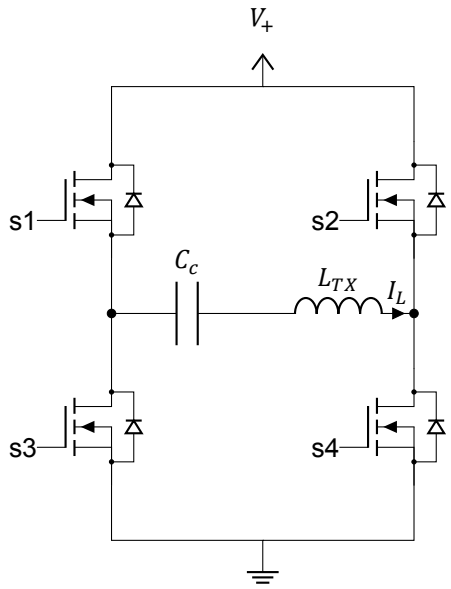

Figure 3.1: Full bridge inverter with transmitting coil.

The output power of the coil can be regulated by altering the frequency and duty cycle of the control signals [17]. The output power is proportional to the duty cycle and inversely dependent on the frequency.

4

Qi Standard

The Qi standard from the Wireless Power Consortium (WPC) is a standard for resonant inductive power transfer for low-power devices. Its Power Class 0 has profiles for ≤5 W and for ≤15 W. The standard describes a system where power is transferred from a base station (wireless charger) to a mobile device.

4.1. Communication

In the Qi standard for wireless charging, communication between the transmitting and receiving devices is facilitated by sending signals throuhg their inductive link. By this method, the receiving device can indicate to the transmitter that it is indeed a chargeable device, how much power it desires to receive, and whether it is done charging. This section describes the specifications for this process set out by the WPC. The focus will be set on the communication protocol from the perspective of the power transmitter, as that is of importance for this project.

4.1.1. Power Transfer Phases

The communication protocol lays out seven phases that the transmitter and receiver progress through in order to set up a stable power transfer [9]. These phases are implemented like states in a finite state machine, where the device's state defines its actions and the inputs define to what state the device may progress.

Making Contact

The transmitter starts in the Selection phase. In this phase, the transmitter uses a small measurement signal sent through the coil to sense objects placed upon the receiving coil. If an object is detected, the transmitter continues to the Ping phase.[9]

In the Ping phase, the transmitter sends out a short power signal through the coil in order to wake up the object if it is a receiver. It then waits for a response from the object. If the transmitter receives a correct response from a receiver, it continues to the Identification & Configuration phase.[9]

Negotiation and Power Transfer

Once contact is made with a receiver the following stages, Identification & Configuration, Negotiation, Calibration, Power Transfer and Renegotiation, deal with obtaining information about the receiver and reaching and maintaining the desired power transmission. Using the information from the receiver, a Power Transfer Contract is created which can be edited throughout power transfer using the different phases. This Power Transfer Contract contains the agreed-upon values that characterize the power transfer that both the receiver and the transmitter use for reference. If in any phase the power transmitter stops receiving correct messages from the receiver, the transmitter stops transmitting power and returns to the Selection phase.[9]

Power Transfer Control

Whether or not enough power is actually reaching the output of the receiver can not be measured by the power transmitter. For that reason, the receiver sends Control Error Packets during the Power Transfer

phase that tell the transmitter by what factor the received power is off-target. This information is then used to calculate the error between the correct transmitter coil current and the current transmitter coil current, which is, in turn, sent through a proportional–integral–derivative (PID) controller to determine a new coil current. Limits are set for the value the integral term of the PID and the PID output can become. These limits and the gain values of the PID controller depend on the used Qi reference design.[9]

4.1.2. Communication Interfaces

The power transmitter and power receiver use different forms of modulation to send messages to the other. The transmitter uses Frequency Shift Keying (FSK), while the receiver uses Amplitude Shift Keying (ASK).[9]

FSK Modulation

As one would expect, the transmitter performs its FSK modulation on the power signal it already sends to the receiver. The transmitter simply switches the transmission frequency between two values to indicate bits of information.[9]

ASK Modulation

On the opposite side, the receiver's ASK modulation does not take place on a signal sent by the receiver itself. Instead, the modulation is also performed on the power signal from the transmitter. The receiver changes the voltage and current in the receiver coil by drawing different amounts of power. Again, by switching this power draw between two values bits of information are communicated.[9]

Bit Encoding

For both directions of information transmission bits are encoded using differential bi-phase encoding. This means that for every ONE bit the modulated signal makes two transitions and for every ZERO bit it makes one transition. Each bit takes exactly one clock cycle with transitions happening on rising and falling clock edges. The clock frequency is defined as $f_{CLK} = 2^{\pm 4\%}$ kHz.[9]

4.2. Foreign Object Detection

The coil current of power transmitters can produce eddy and induced current inside certain objects, which can, in turn, lead to a quite significant power loss in the form of heat [9]. It is thus important that the transmitter can detect whenever these types of foreign objects are placed near the transmitter and respond accordingly. Which will usually mean ceasing the transmission of power. The Qi standard presents two protocols to implement for such Foreign Object Detection (FOD).[9]

Quality Factor Change

FOD based on quality factor change is the standard FOD method used by 15 W wireless power transmitters. The transmitter measures the quality factor of the coil after a receiver is placed in position during the Selection phase, but before making contact with the receiver. Then, during the Negotiation phase, the receiver sends the reference quality factor to the transmitter, which is the quality factor of a universal test transmitter's coil if this specific receiver is placed upon it. The transmitter has to account for the difference between its own coil and that of the test transmitter to determine what the quality factor should be without a foreign object and choose a threshold value for the quality factor accordingly. If the quality factor at any point surpasses this threshold, the transmitter will return to the Selection phase, and thus stopping power transfer.[9]

Calibrated Power Loss Accounting

Another simpler method of FOD is determining the power loss. In this protocol, the receiver continuously updates the transmitter on the power at its output. The transmitter can then simply compare this power to the power it is transmitting and determine if too much power is lost into foreign objects.[9]

4.3. Qi Reference Design

The Qi standard has several reference designs that are recommended [9]. To accomplish 15 W, a medium power (MP) design has to be chosen. Several designs are compared in table 4.1. The reference design "MP-A2" was chosen because of two reasons. Firstly, the absence of voltage/phase

control and use of a single coil allow for a more straightforward design. The second reason was the availability of a controlling integrated circuit (IC) for this design. This would allow for a straightforward and compact design.

Table 4.1: Reference designs with several parameters.

Design	Input voltage [V]	Voltage control	Phase control	Coils
MP-A1	19	No	Yes	1
MP-A2	12	No	No	1
MP-A3	2.5–11.5	Yes	No	1
MP-A4	12	No	Yes	1
MP-A5	1–12	Yes	No	1
MP-A6	1–18	Yes	No	3
MP-A7	19	No	Yes	1
MP-A8	12	No	Yes	3
MP-B1	15	No	Yes	4

5

Power Conversion

The wireless power transmitter uses a coil that is powered by a 12 V AC signal to transmit power to a receiver. This is decided by the reference design selected in section 4.3. Meanwhile, the entire transmitting unit is powered by batteries that, over the course of operation, will vary in voltage. This chapter covers the design of that power conversion circuitry, which entails the conversion of the DC battery voltage input to the 12 V AC signal to drive the transmitting coil. The circuit will consist of two parts, a voltage regulator that will maintain a steady voltage, and an inverter to convert from DC to AC.

5.1. Voltage regulator

According to the MP-A2 reference design from the Qi standard that was selected in section 4.3, the transmitting coil should be driven with a signal with an amplitude of 12 V. However, the DC input voltage received from the battery will have a certain range depending on the characteristic of the battery. This requires a voltage regulator, but first, section 5.1.1 discusses what this input voltage range will be.

5.1.1. Battery Voltage Range

Batteries are made of cells that can be connected in series and in parallel to create a battery with the desired voltage and current characteristics. Different types of battery cells also have different individual voltages. These choices are made by the battery management system [1]. However, the battery voltage chosen is also important for the wireless charging system. More specifically for the voltage regulator discussed here. This is why it was determined that the lower bound of the battery voltage should be 15 V. Firstly, at this frequency, a simpler step-down voltage regulator can be used. Secondly, by maintaining a margin from the desired 12 V the voltage regulator never has to perform a very small voltage drop, which is more difficult for the regulator to do. And lastly, 15 V coincides with the lower voltage boundary of 5 lithium-ion cells connected in series. More on this is described by the battery management system [1]. For the converter, it is important to know that the battery input voltage will range from 15 to 21 V.

5.1.2. Buck Converter

There exists a wide range of possible converter topologies that can step down the voltage. To determine the best ones for implementation within the Powerlizer the most important metrics are size and efficiency. The size metric rules out isolated converters, as their transformers always lead to larger sizes than their non-isolated counterparts. Within non-isolated converters, there are still lots of options, like buck, boost, Ćuk, Zeta, and SEPIC converters. However, when the application only requires stepping down the voltage at low power, the buck converter stands out as the most power-efficient while also being the least complex topology [18].

Figure 5.1 shows the general schematic of an asynchronous buck converter. The way a buck converter achieves a lower output voltage than its source is by using a MOSFET and a diode to alternatingly connect and disconnect the source from the load. When the source is connected, current starts flowing through the inductor into the capacitor and through the load. As the current comes closer to the steady-state value, the voltage across the inductor decreases and the voltage across the load increases

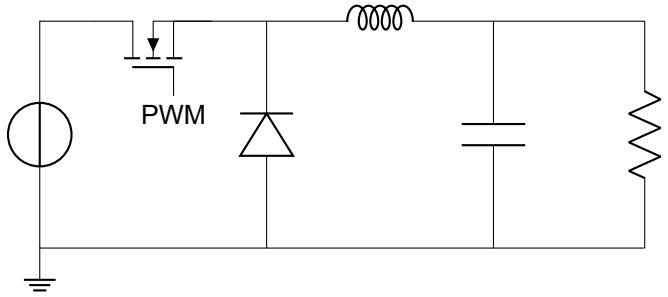

Figure 5.1: Buck converter schematic

towards the source voltages. However, to maintain the lower load voltage the source is disconnect before a steady state is reached. Now, the inductor and capacitor will maintain the voltage across the load, transferring the energy they stored as magnetic field and electric charge respectively when the source was connected in the load. By switching between these connected and disconnected states at a high frequency, a steady output voltage can be maintained. This also depends on the inductance and capacitance of the inductor and capacitor. Higher values for both will result in a slower change in the output voltage. This means less ripple in the output voltage, but also a longer startup time for the circuit.

The actual level of the output voltage depends on the duty cycle of the signal controlling the MOSFET, which determines the fraction of the time the MOSFET is closed versus open. The output voltage is determined by the duty cycle according to equation 5.1.

$$V_{out} = DV_{in} \tag{5.1}$$

This ripple voltage is an important metric if the buck converter has to function as a stable voltage supply. If the average output voltage V_{out}, the inductor, and the capacitor are known, the output voltage ripple can be approximated [19]. The output voltage ripple is the same as the ripple in the capacitor voltage, which is in turn dependent on the fluctuation of the charge within the capacitor following equation 5.2.

$$\Delta v_C = \frac{\Delta Q}{C} \tag{5.2}$$

This charge difference ΔQ is determined by the ripple in the capacitor current. When the converter has reached its steady-state operating point, the output voltage and current are constant. This means that the capacitor current follows equation 5.3.

$$i_C(t) = i_L(t) - I_{out} \tag{5.3}$$

This means that the current ripple in the capacitor is equal to that in the inductor. Therefore, the next step is to calculate the inductor current ripple.

The inductor current of a buck converter at a steady operating point follows the simple scheme of increasing when the converter's MOSFET is closed and decreasing an equal amount when the MOSFET is open. Therefore, to determine the inductor current ripple, only one of two states has to be analyzed. Figure 5.2 shows the buck converter circuit with the MOSFET open.

With V_{out} constant, V_L is also constant. Equation 5.4 then shows that the inductor current will have a constant rate of change.

$$V_L = L\frac{di(t)}{dt} \tag{5.4}$$

Equation 5.5 is then obtained as an expression for the change rate of the inductor current.

$$\frac{di(t)}{dt} = \frac{V_L}{L} = \frac{V_D + V_{out}}{L} \tag{5.5}$$

Finally, the inductor current ripple is simply this current change sustained over the time that the MOSFET remains open. This depends on the duty cycle and the switching frequency of the MOSFET. The inductor current ripple is therefore expressed as in equation 5.6

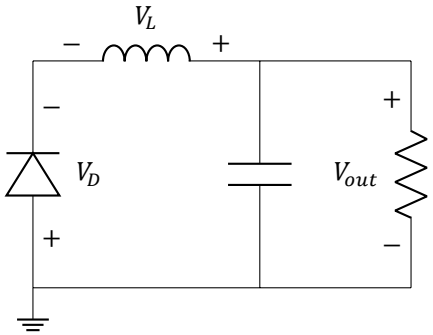

Figure 5.2: Buck converter schematic with its MOSFET open

$$\Delta i_L = \frac{V_D + V_{out}}{L} T_{open} = \frac{V_D + V_{out}}{L}(1 - D)\frac{1}{f_{sw}} = \Delta i_C \tag{5.6}$$

Here T_{open} is the time the MOSFET remains open in one operation cycle and D is the duty cycle.

The charge fluctuation in the capacitor resulting from the current ripple through the capacitor is expressed by equation 5.7. This is derived in appendix B.4.1.

$$\Delta Q = \frac{1}{8}\frac{\Delta i_C}{f_{sw}} \tag{5.7}$$

Equation 5.2, 5.5 and 5.7 result in output voltage ripple equation 5.8

$$\Delta v_{out} = \frac{(V_D + V_{out})(1 - D)}{8LCf_{sw}^2} \tag{5.8}$$

5.1.3. Requirements

Table 5.1 shows the most important specification requirements for the buck converter design.

To start, the input and output voltage requirements are the results of the possible input voltages coming from the batteries and the (12 ± 1) V output required for the wireless power transfer. This was already explained in the introduction of this chapter. The margin of 1 V for the output voltage originates from the Qi standard [9] and gives an absolute limit of 2 V for the output voltage ripple.

Next, the third requirement, an output current of up to 2.5 A, is a result of the power that the buck converter should be able to deliver. System requirements [**M.2**] and [**M.3**] lead to a possible power draw of 30 W, which, at 12 V, means a current of 2.5 A.

The switching frequency requirement was already mentioned as system requirement [**T.2**]. The switching of the MOSFET in the buck converter will produce noise around the switching frequency and harmonics at higher frequencies [20]. This noise can negatively affect communication with a power receiver if it is inside the frequency range of this communication. It is therefore required that the switching frequency is above this range.

The final two requirements are the result of the buck converter's application on the Powerlizer. Due to limited energy available in the batteries, it is very important that the converter has as little losses a possible. This is also reflected in system requirement [**M.3**]. And finally, to adhere to system requirement [**SO.3**], a small size for all components should be striven towards.

Table 5.1: Buck converter specifications

Parameter	Specification
Input voltage	15–21 V
Output voltage	(12 ± 1) V
Output current	2.5 A
Switching frequency	>200 kHz
Power efficiency	High
Size	Small

5.1.4. Design

The aforementioned requirements for the buck converter in this wireless charging module are quite simple and common. Therefore, there are a lot of ICs on the market that can be adopted in the implementation of this converter and help to keep the final design compact in size. For this project, the TPS84250RKGR switching voltage regulator was selected. It has an integrated coil, which can decrease the complexity of the PCB design and it has a high efficiency of around the 92 % for this application.

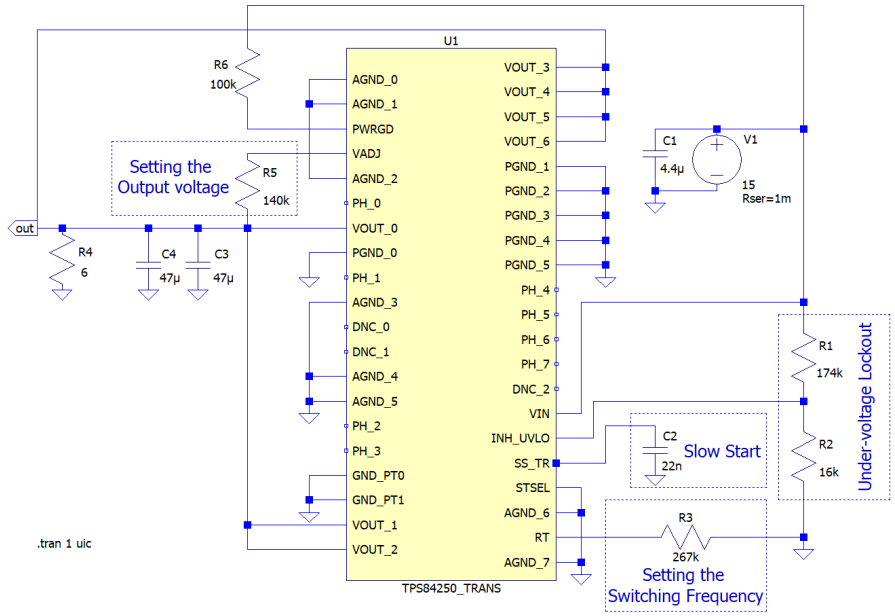

Figure 5.3: LTspice buck converter circuit.

Under-voltage Lockout

R1 and R2 form a voltage divider to configure the under-voltage lockout. The INH_UVLO pin connects to the shutdown logic inside the IC. This allows the buck converter to shut itself off if the input voltage is too low to produce a stable output at the desired voltage. According to the IC's datasheet resistances of 147 kΩ and 15.8 kΩ for R1 and R2 respectively results in a threshold voltage of 15 V, which is the lowest desirable input voltage of wireless charging module and also the lowest voltage at which the buck converter can produce 12 V. However, in simulations of the buck converter circuit, it was observed that with the aforementioned resistor values the converter shut-off happened at input voltages above 15 V. Therefore, the value of R2 was adjusted to 16 kΩ, which allows for good performance at 15 V as presented in section 5.1.6.

Setting the Output Voltage

R5 sets the output voltage of the converter. Inside the IC there is a second resistor that, together with R5, forms a voltage divider. The voltage out of this divider is fed to a comparator inside the IC, which informs the switching circuitry whether the desired output has been reached. A resistor of 140 kΩ for resistor R5 leads to the desired output voltage of 12 V.

Setting the Switching Frequency

The value of R3 determines the switching frequency. The manufacturer recommends a switching frequency of 800 kHz for an output voltage of 12 V. This corresponds to a value of 247 kΩ for R3.

Slow Start

Capacitor C2 provides an additional capacitance for the slow start. The capacitor is slowly charged, increasing the voltage on it. That voltage is fed to the comparator that determines the output voltage. This makes the buck converter take more time to reach a 12 V output, thus limiting the amount of current drawn during startup to charge the output capacitors. The IC already contains a capacitor for a slow start, but for high output voltage, an additional capacitor is desirable to slow down startup even more.

Output Voltage Ripple
Capacitors C4 and C3 function as the output capacitors of the buck converter and influence the output voltage ripple. By filling these capacitor values, the 4.7 µH inductance within the IC, the 800 kHz operating frequency, and a simple duty cycle following equation 5.1 into voltage ripple equation 5.8, a voltage ripple of 1.12 mV is obtained.

5.1.5. 5V USB Output
The capability to charge a device using a USB cable was added in the form of a female USB type A port to follow requirement [**SF.2**]. This port is supplied with a 5 V 2.5 A buck converter, similar to the 12 V converter. The data pins (D+ and D-) of the USB port will be shorted to signal the charging device that it is a USB Battery Charging 1.2 Dedicated Charging port. To comply with this standard, the output voltage should be in the range of 4.75–5.25 V and the maximum current that may be supplied is 5 A [21].

The 5 V buck converter of the USB port uses the same IC as the 12 V buck converter. The IC was selected to also have the ability to output 5 V as this would decrease design complexity. The layout of the 5 V buck converter circuit is the same as Figure 5.3 except no slow start capacitor is included. Besides this, resistance values have been changed to reconfigure the buck converter IC. First, R2 is changed to 31.6 kΩ to raise the under-voltage lockout. Next, R5 is lowered to 52.3 kΩ to set the output voltage. Finally, R3 is set to 1.1 MΩ to lower the switching frequency to 500 kHz. The USB standard allows for less ripple on the output voltage, only allowing an absolute max of 0.5 V. However, for the 12 V buck converter this ripple was only 1.12 mV and according to equation 5.8 the output ripple at 5 V is even smaller.

5.1.6. Simulation
The buck converter circuit design in Figure 5.3 was simulated in LTspice. The input voltage was set to 15 V, the lowest value at which the converter should still operate, and the load was set to 6 Ω such that a considerable current of 2 A is drawn.

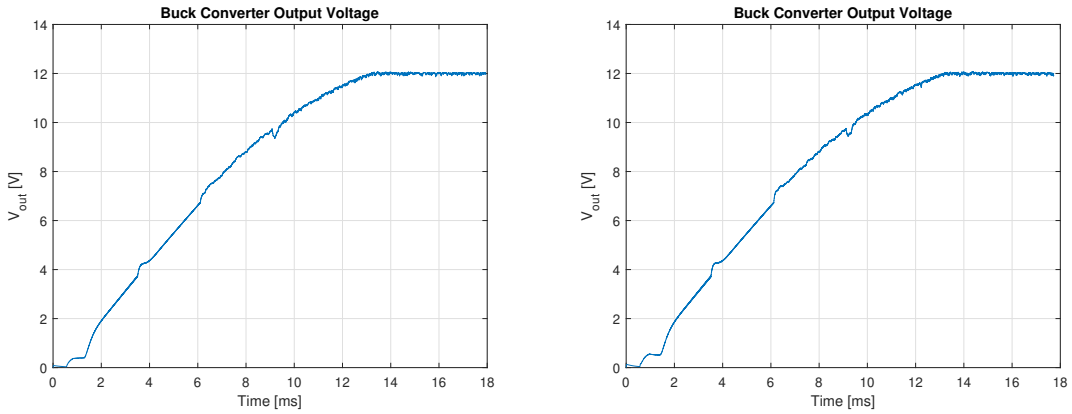

(a) 15 V input and 2 A output

(b) 21 V input and 2.5 A output

Figure 5.4: Buck converter output voltage obtained from LTspice simulation circuit in Figure 5.3

Figure 5.4a plots the output voltage of the buck converter during startup. The circuit behaves as desired. Most importantly, the 12 V output is reached and it takes less than 14 ms for the converter to reach and maintain the 12 V output. The voltage ripple in simulation is larger than obtained from circuit analysis at 13 mV, however from a larger fluctuation in the output voltage of 180 mV is present that seems to be due to the behavior of the buck converter IC's control system. This fluctuation does also remain within the bounds specified in section 5.1.3.

The same can be concluded from Figure 5.4b, which results from a simulation with a input voltage of 21 V and an output current of 2.5 A. When comparing Figure 5.4a and Figure 5.4b it can be assumed that the startup behavior of the buck converter does not depend on the operating conditions within the specified range and also at an output of 5 V.

In Figure 5.4a, after having reached the steady output voltage, the converter draws 25.25 W from the source, while delivering 24.00 W to the load. This means that the power efficiency of the buck converter

under these conditions is 95.0 %. In Figure 5.4b, the converter draws 31.65 W from the source, while delivering 30.00 W to the load. This means that the power efficiency of the buck converter under this second set of conditions is slightly lower at 94.8 %.

For buck converters, power is mostly lost due to the ESR of the inductor and the capacitor and due to the conduction and switching losses of the MOSFET. While no circuit analysis could be performed to estimated power efficiency due to the lack of specifications for the components within the converter IC. The efficiency obtained is to be expected based on the data sheet of the IC. Buck converters have fewer losses when the voltage drop required is small, because the load spends more time directly connected to the source. Therefore, with the small voltage drop required for wireless charging system, the efficiency should be close to the IC's maximum efficiency of 96 %.

5.2. Inverter

Transferring power between two coupled coils requires the primary coil to be supplied with an AC signal. However, batteries, by which the wireless power transmitter is powered, supply a DC voltage. This is why an inverter needs to be designed to convert the power from the batteries from DC to AC.

5.2.1. Full-bridge Inverter

Disregarding any mechanical inverter topologies for their low efficiency, there are still a lot of inverter types that are entirely electronic that could be implemented. Most of these use MOSFETs to perform their switching actions, but by harnessing different topologies their characteristics can be very different. [22] presents a wide range of inverter types. One key distinction in these is whether the inverter outputs a square wave of a sine wave. For this project, a square wave inverter is used, because square wave inverters have a much simpler circuit and are much cheaper to implement. Besides this, the load of the inverter, in the form of the transmitting coil and compensation, will form a resonant circuit that filters out most frequencies outside of the resonant frequency and limits the effect of the inverter's noise on the receiver. A very commonly used topology is the full-bridge (or H-bridge) inverter. In applications like the Powerlizer, where the voltages are low and no increase in the voltage is needed, these can be a very simple, cheap and small implementation of an inverter. This is why a full-bridge inverter is to be designed for this wireless power transmitter and why the MP-A2 reference design chosen in section 4.3 also dictates this. Theoretical background on the full-bridge inverter was covered in section 3.2.2.

Worth mentioning is that the MP-A2 standard also uses its full-bridge as a half-bridge inverter for certain tasks. A half-bridge inverter has much the same behavior as the full-bridge counterpart and evidently can also perform the same job for wireless power transfer, but they do not make full use of the available voltage [23]. They only connect the input voltage to the output in one direction, which results in half the voltage swing and thus a quarter of the output power.

5.2.2. Full-bridge Gate Driver

To drive the gates of the full-bridge inverter, a gate driver is needed. Firstly it is needed to turn the high-side switching NMOS transistors on when the switching node is at the supply voltage. This is done by bootstrapping. Secondly, the gate driver is needed to deliver higher currents than a microcontroller can deliver.

Bootstrap

By using a capacitor that follows the source voltage of the MOSFET and a diode connected to the supply voltage, a threshold voltage between the gate and source can be reached. This way, a transistor can turn on even when the bridge voltage is higher than the supply voltage.

Gate Resistor

A gate resistor is added to reduce ringing. The gate capacitance and the inductance of the trace driving it can form an oscillator. When this circuit oscillates, the transistor can have a higher impedance. This will cause unwanted behaviour and losses.

Pull-down Resistor

When the transistors are not in use, they should be turned off. This can be easily accomplished by inserting a high resistance resistor between the gate and the source. This way, the gate to source voltage becomes 0 V when the gate is not driven and thus the transistor will be off.

5.2.3. MOSFET Requirements

The Full-bridge inverter that is to be designed solely consists of 4 MOSFETs and the control signals from the Qi IC discussed in section 6.1.1. The inverter is supplied with 12 V from the buck converter covered in section 5.1 above and outputs to the coil and compensation discussed in section 6.1.3. This is why the inverter requirements immediately lead to the MOSFET specifications in table 5.2.

Table 5.2: Inverter MOSFET specifications

Parameter	Specification
Drain-Source Breakdown Voltage	>12 V
Continuous drain current	>2.5 A
Switching frequency	110–145 kHz
Power efficiency	High

A simple first requirement is that each MOSFET should handle the input voltage. This results in the requirement that the Drain-Source Breakdown Voltage of the MOSFETs should be larger than 12 V. It is of course important to at least maintain a margin of 30 % for this specification.

The next requirement results directly from the 12 V amplitude, the 15 W power requirement [**M.2**] and the 50 % power efficiency requirement [**M.3**]. The inverter should be able to maintain 2.5 A of current running through it to deliver the required power. This translates to a continuous drain current specification of 2.5 A.

The third requirement specifies at what frequencies the inverter, and thus the MOSFETs, should switch. These frequencies are 110–145 kHz, as specified by the Qi reference design selected in section 4.3, and will be maintained by the Qi IC. The absolute maximum switching frequency of a MOSFET is determined by adding its turn-on delay time, turn-on rise time, turn-off delay time, turn-off rise time and reverse recovery time to obtain the switching time. However, most modern MOSFETs can switch orders of magnitude faster than required for this application, so this requirement does not need much attention.

The final thing to pay attention to in selecting MOSFETs is to optimize for power efficiency. This efficiency is mainly determined by two factors: conduction and switching losses. The first is determined by the on-resistance. Therefore, to minimize losses, the on-resistance of the MOSFETs should be as low as possible. The switching losses are mostly determined by how quickly the switching happens, which is determined by the rise time, fall time and the reverse recovery time [24]. So, these values should also be low for the selected MOSFETs.

5.2.4. MOSFET Selection

A full-bridge inverter can be made using four MOSFETs. These MOSFETs should switch at a sufficiently high frequency and have a low on-resistance to minimize power loss and maximize efficiency. The DMG7430LFG from Diodes Incorporated was recommended in the datasheet of the Qi compliant IC [25]. This MOSFET was not available at the time of the project so a different MOSFET was used. In particular, the DMHT3006LFJ from Diodes Incorporated was chosen for its low on-resistance and it featured the correct voltage specifications. This component has four identical MOSFETs integrated in one IC, which costs less than four seperate MOSFETs.

Table 5.3: Selection of MOSFETs available on the market.

MOSFET	$V_{(BR)DSS}$ [V]	I_D [A]	$R_{DS(on)}$ [mΩ]	t_r [ns]	t_f [ns]	Price [€]
DMHT3006LFJ	30	13	7.8	54	4.3	1.13
DMG7430LFG	30	10.5	11	21.2	5.1	1.52
PMV100ENEA	30	3	70	6	4	1.05
DMHT6016LFJ	60	8.7	22.2	5.2	7	1.47

Simulation of the inverter design will be covered in section 6.2.

6

Control and Transfer

Besides the power conversion components, there are several other subsystems present in the wireless charging system. A coil with compensation is needed for magnetic resonance charging. The Qi standard communication needs to be received and decoded too. A simulation of this system will be done in LTspice and lastly, a conceptual design of (a part of) the Powerlizer's high-level controller will be presented.

6.1. Qi Wireless Charger Design

For the wireless charging part of the system, an IC was chosen to control the full-bridge inverter. The coil and compensation were also chosen according to the Qi standard.

6.1.1. Wireless Charging IC

The P9242-R from Renesas [25] was used to handle the communication and control of the Qi standard. It features a processor, several regulators, an ASK detector, and gate drivers for the full-bridge inverter. Along with this IC and its complementary components, there are several other subsystems that need to be designed. A 12 V regulator is used to power the IC and its internal regulators. The full-bridge driving outputs are connected to the full-bridge inverter which in turn is connected to the coil and its compensation. All these subsystems will be incorporated on a PCB which will be described in Section 7.1.

Communication

The IC measures the current and voltage of the coil to detect the ASK communication signal of the receiver. One or the other is chosen depending on whether current sensing or voltage sensing produces a better demodulated signal. An envelope detector was needed outside of the IC. Based on the detected bits, the controller adjusts the frequency and duty cycle of the inverter. It does so as outlined in Section 4.1 and the Qi standard [9]. It will communicate back to the receiver by changing the frequency of the full-bridge around the operating frequency with an FSK signal.

Fault Protection

Several fault protection measures are implemented in the IC. The current can be limited using external resistors. The current limit was set to 2.5 A as that was recommended by the manufacturer for 15 W applications [25] and this was also the current limit of the buck converter. The temperature of the coil can be monitored by a thermistor to avoid overheating. It also features under-voltage lockout to ensure correct operation. The Q-factor is also measured to detect foreign objects. A buzzer will beep when this is the case. LEDs outside of the IC will indicate the state of the power transfer as well as if the chip detects any faults.

6.1.2. Coil Design

Coil Dimensions

The dimensions of the transmitting coil are fixed by the reference design. These dimension can be found in Figure 6.1. The coil is made of 12 turns of 17 AWG Litz wire having 105 strands of 40 AWG. Litz wire is used because at higher frequencies, the current through a wire runs mostly across the surface.

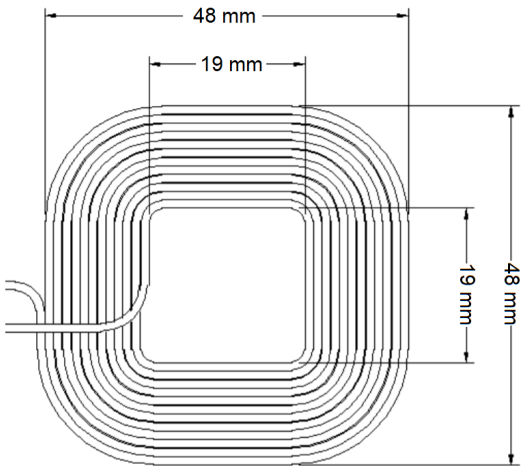

Figure 6.1: Dimensions of the transmitting coil for the MP-A2 standard [9].

The skin depth marks the point where the current density has fallen to $1/e$ of its value on the surface [13]. The formula to calculate the skin effect can be seen in equation 6.1. The 40 AWG strands are 0.08 mm in diameter so there will be significant current density in the whole strand since the skin depth is 0.172 mm for a copper wire at a frequency of 145 kHz (maximum operating frequency of the MP-A2 design). With a bigger strand, this will not be the case. By combining multiple strands, the resistance of the coil can be reduced to have lower losses and a higher current capability.

$$\delta = \frac{1}{\sqrt{\pi\sigma\mu f}} \approx 0.172\,\text{mm} \tag{6.1}$$

The AC resistance of the coil can be calculated by equation 6.2. Here R is the resistance [Ω], ω is the angular frequency [rad], L is the inductance [H] and Q is the quality factor [-]. At a frequency of 145 kHz, this resistance will be 65 mΩ.

$$R = \frac{\omega L}{Q} = 65\,\text{m}\Omega \tag{6.2}$$

Proximity Effect

Besides the skin effect, there is also the proximity effect influencing the AC resistance of the coil [13]. The proximity effect is caused by the magnetic field from each strand influencing the current density in other strands [26]. By dividing the conductor height by the skin depth, a factor between the AC resistance and DC resistance can be read from a graph. As a result of the skin depth being about twice the conductor height and because there was only one layer, the proximity effect did not influence the AC resistance too much.

Magnetic Simulation

A magnetic field simulation was performed on an simplified TX-RX system. The result can be seen in Figure 6.2.

Here, the coil of the MP-A2 transmitter design was used and the receiving coil of the power receiver example 4 (15 W) [9]. The current in the primary coil was set to 2.5 A and there was no current in the

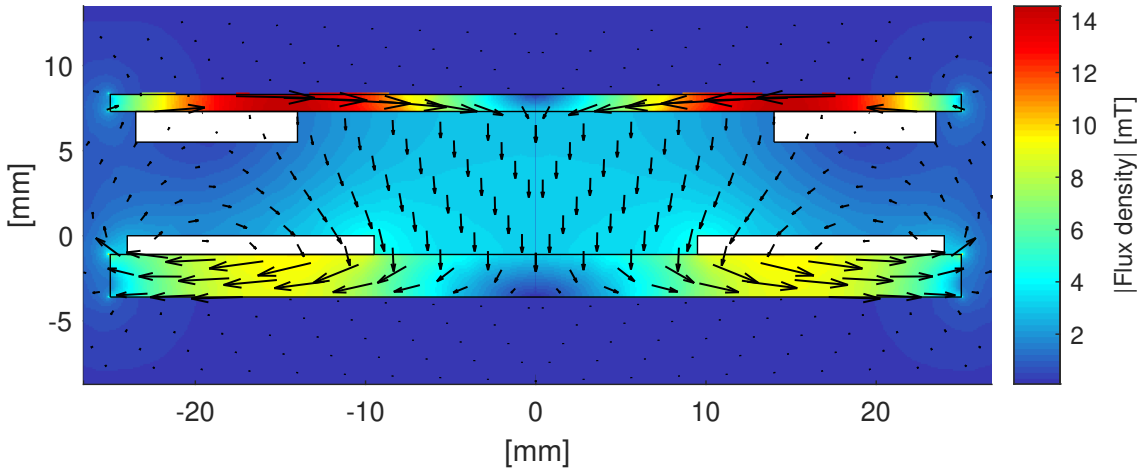

Figure 6.2: FEMM simulation of the transmitting- and receiving coil.

secondary coil. On the top, a cross-section of the two-layer receiving coil can be seen in white. A cross-section of the transmitting coil can be found on the bottom. The shielding on both sides is outlined in black. The magnitude of the flux density is plotted in color and the magnitude of the magnetic field is plotted by the vectors.

The coils were approximated to be circular. From this analysis, the coupling coefficient can be calculated. A coupling coefficient of 1 means that all of the flux is coupled, and 0 means that no flux is coupled. As can be seen from Equation 6.4, the coupling coefficient of the simulated system is 0.63. In this equation, M [H] represents the mutual inductance, ϕ_{RX} [Wb] the flux through the receiving coil, and I_{TX} [A] is the current through the transmitting coil. L_{TX} [H] and L_{RX} [H] are the inductances of the transmitting and receiving coil respectively.

$$M = \frac{\phi_{RX}}{I_{TX}} \approx 13.4\,\mu\text{H} \tag{6.3}$$

$$k = \frac{M}{\sqrt{L_{TX}L_{RX}}} \approx 0.63 \tag{6.4}$$

The magnetic field strength at a distance of 10 m from the centre of the coil was measured from the simulation. This came out to be -27 dB µA/m, which is well within the legal limits (42 dB µA/m) [27]. This means that requirement [**S.1**] will most likely also be satisfied.

6.1.3. Compensation Design

To compensate the primary coil, series compensation was used, see Section 3.2.1. The value given in the Qi standard is 247 nF while in the datasheet of the IC a value of 215 nF. This will result in different resonance frequencies ($f_0 = \frac{1}{2\pi\sqrt{LC}}$) with the 10 µH coil. Namely, 101.3 kHz for the Qi standard and 108.5 kHz for the IC.

This circuit was analyzed in Section B.4.2. The input voltage was square wave with an amplitude

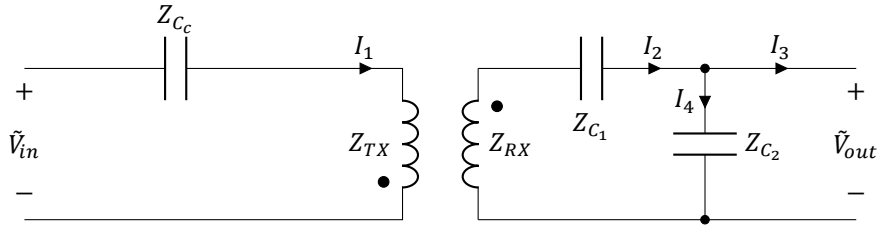

Figure 6.3: Equivalent circuit of the primary- and secondary coil and compensation.

of 12 V. The output should be rectified to 12 V so its amplitude should be $\frac{12\pi}{2}$ before rectification.

$$
\begin{aligned}
M &= 13.4\,\mu\text{H} \\
V_{in} &= 12\,\text{V} \\
V_{out} &= \frac{12\pi}{2}\,\text{V} \\
\omega &= 2\pi \cdot 110 \cdot 10^3\,\text{rad/s}
\end{aligned}
$$

The capacitors were approximated to have a series resistance of 10 mΩ. By filling in the following values for the components, an efficiency can be calculated for both of the capacitor values:

$$
\begin{aligned}
Z_{TX} &= 65 \cdot 10^{-3} + j\omega 10 \cdot 10^{-6}\,\Omega \\
Z_{RX} &= 0.9 + j\omega 44.8 \cdot 10^{-6}\Omega \\
Z_{C_{c1}} &= 10 \cdot 10^{-3} + \frac{1}{j\omega 247 \cdot 10^{-9}}\,\Omega \\
Z_{C_{c2}} &= 10 \cdot 10^{-3} + \frac{1}{j\omega 215 \cdot 10^{-9}}\,\Omega \\
Z_{C_1} &= 10 \cdot 10^{-3} + \frac{1}{j\omega 56 \cdot 10^{-9}}\,\Omega \\
Z_{C_2} &= 10 \cdot 10^{-3} + \frac{1}{j\omega 0.8 \cdot 10^{-9}}\,\Omega
\end{aligned}
$$

The efficiency for the 247 nF came out to be 86.5 % while the efficiency for the 215 nF was only 75.6 %. This would make the 247 nF a better choice for the compensation and it was incorporated into the design.

6.2. Equivalent Circuit Model Simulation

For the power transfer part of the circuit, an equivalent model was created in LTspice. Two coils were coupled with the coupling coefficient from the FEMM simulation. The compensation was added on both sides as described in part 4 of the Qi standard [9]. The output was rectified and loaded with a 12 V DC source. This source is the result of the receiver communicating to the transmitter to regulate the output to 12 V. The input was approximated by a 12 V DC source, as this was approximately the case in the simulation in Section 5.1.6. The full-bridge inverter was modeled by using the DMHT3006LFJ MOSFET model [28]. The gate drivers were approximated by a 5 V pulse source with a frequency of 125 kHz and a duty cycle of 40 %. The schematic can be seen in Figure 6.4.

The efficiency of the system can be calculated by dividing the output power by the input power of the circuit in Figure 6.4. The input power is the power coming out of V5 and the output power is the power going into V6. The power is measured by multiplying their respective currents with their voltage. By averaging both of those values over time (in the steady state after 100 µs), an efficiency of 78 % was obtained. The output power was 14.9 W at an input power of 19.2 W. Of this power, around 332 mW was dissipated in the full-bridge inverter. The rectifier circuit on the secondary side dissipated around 1849 mW. This left a power loss of 2119 mW in the magnetic circuit. By including a converter efficiency of 95 %, the total efficiency of the system will be 74 %. This is well over the required efficiency set in requirement [**M.3**]. The distribution of the power losses can be found in Figure 6.5.

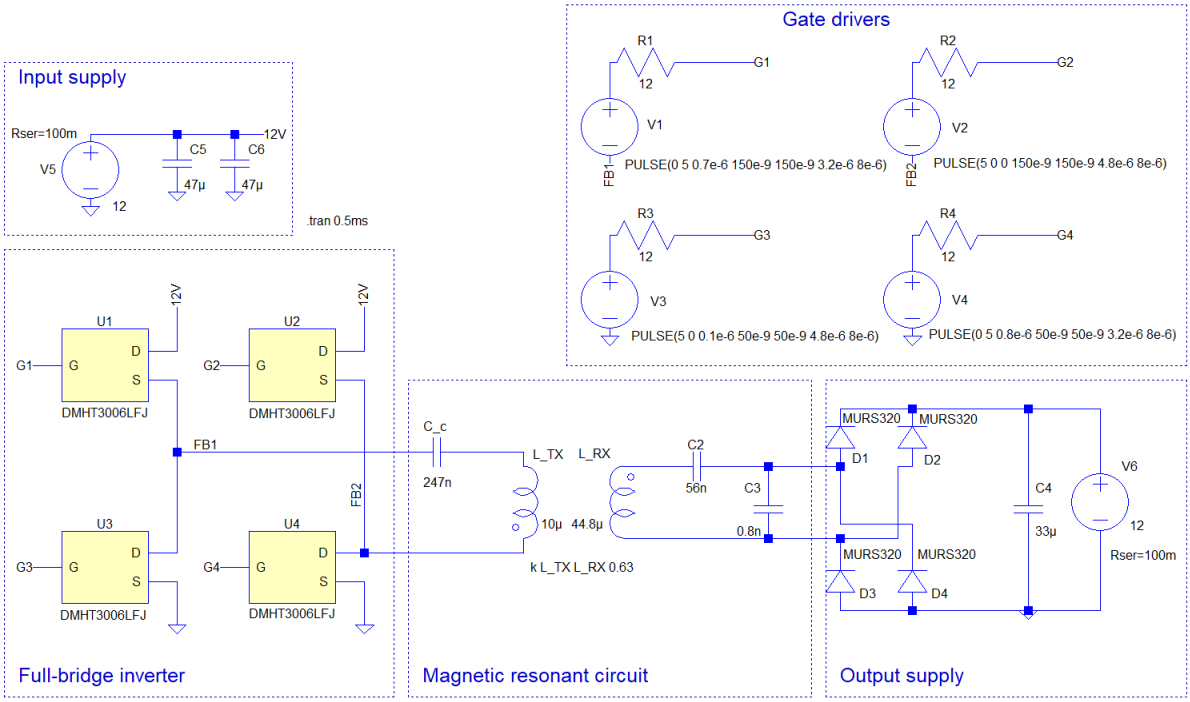

Figure 6.4: LTspice equivalent circuit.

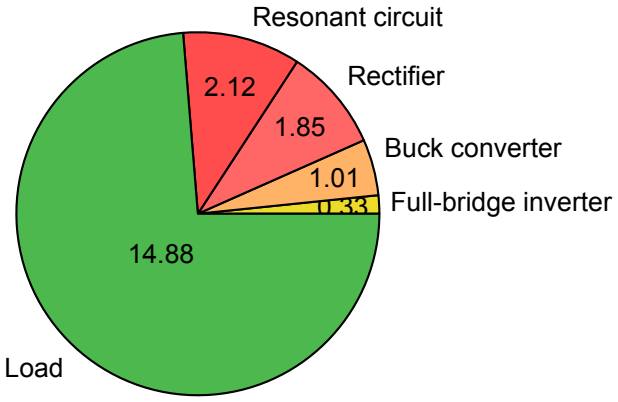

Figure 6.5: Power distribution in W.

6.3. High-level Controller

To control all three separate systems of the Powerlizer, a high-level controller could be implemented. This controller can be used to turn the wireless charging system on or off and it can read out the outputs of the system. In this section, a conceptual design will be presented that is not part of the prototype.

6.3.1. I2C Communication

The Qi IC provides an I2C output that can be read out by the high-level controller. In this way, the state (startup, idle ping, power transfer, etc.), status (system normal, FOD alarm, over-current, etc.), and the coil current among others can be read out [25]. The high-level controller can then make decisions by requesting information from the right address.

6.3.2. Enabling and Disabling the Charger

To save power, the wireless charging system could be turned off when the lid is closed and there is no wireless charging device inside. The high-level controller could determine this by reading the state register using the I2C interface when it detects that the lid has closed. If there is power transfer

happening when the lid is closed, the wireless charger should stay on. If it is still idle, the wireless charger can be turned off so it does not ping anymore and thus consumes less power. This can be accomplished by pulling the Enable pin of the P9242-R high (more than 2.5 V). The system should be turned on again when the lid is opened. It is assumed that if there is no power transfer happening at the moment the lid closes, the wireless charging device is not properly aligned or not present at all. Then, the wireless charger can be turned off. Even if the wireless charger is not turned off, it consumes only 1 mA when idle. However, if the IC is turned off, it only uses a few tens of µA. A sensor to detect the lid opening and closing is already needed for the disinfection system. The voltage converters can also be turned off by the controller by putting a transistor in parallel with R2 in Figure 5.3. By turning the transistor on, the under-voltage lockout will be pulled low and the buck converter will turn off.

6.3.3. Clock Synchronization

To reduce the noise on the power lines, the converters could be synchronized to be out of phase with each other. This can be done by providing a clock signal to the RT pin in Figure 5.3. By having the frequencies out of phase, the voltage- and current ripple will destructively interfere. This will reduce the noise in the system and its electromagnetic radiation.

7 Prototype

A PCB was assembled with the components outlined in the design Chapter 5 and Chapter 6. With this prototype, mobile devices can be charged either using a wire, or wirelessly. The input consists of two wires, which can be connected to a 15–50 V DC source to power the circuit. The outputs consist of a female USB type A port, a wireless charging coil, output voltage ports, and ”power good” flags of the converters, and an I2C interface to the main IC.

7.1. PCB design

A PCB was designed in KiCAD to connect all the components in a small area. The recommendations of the manufacturers of the Qi IC [25] and the voltage regulators [29] were followed. The complete schematic can be seen in Appendix B.3. This schematic was converted to a PCB layout by downloading the appropriate footprints from mouser.com for the non-standard components. For the passive components, mostly 0603 SMD hand solder footprints were used to save space but still be able to solder them by hand. The two copper layers can be seen in Figure 7.1. Power-carrying traces were made wider to decrease their resistance. This will ensure that the traces can carry the high currents without heating up too much. To dissipate the heat from the ICs, thermal vias were added underneath them. This will create a copper connection to the ground plane on the underside that will act as a heatsink. Two separate ground planes were added; one for the power signals and one for the more sensitive signals. This will ensure that the high current of the power lines will not create a voltage difference between the ground connections of the sensitive signals, like the current sensing circuitry. This difference in ground potential would create noise in the circuit which would lead to unnecessary errors in the measurements. These ground planes were connected underneath the buck converters as advised by their datasheet [29]. Test pads were used to be able to solder wires to the input- and output ports.

7.1.1. Manufacturing

The PCB was manufactured on a two-layer FR-4 board with 1 oz/cm^3 copper. The height of the copper layers was 35 µm. A stencil for the solder paste application was also manufactured. Their holes were reduced by 10 % compared to the exposed copper pads to reduce the amount of excessive solder.

7.1.2. Assembly

To assemble the PCB, solder paste was applied on top of the exposed pads. The components from the BOM list were then placed on their appropriate pads using tweezers. This list can be found in Appendix B.3. During the assembly, several errors were found in the trace connections. These were fixed by adding wires over the top of the PCB and angling the components off of their designated pads. An updated schematic without these errors can be found in Appendix B.3. The dimension of the PCB are 81 mm by 46 mm. This can thus satisfy requirement [**SO.3**].

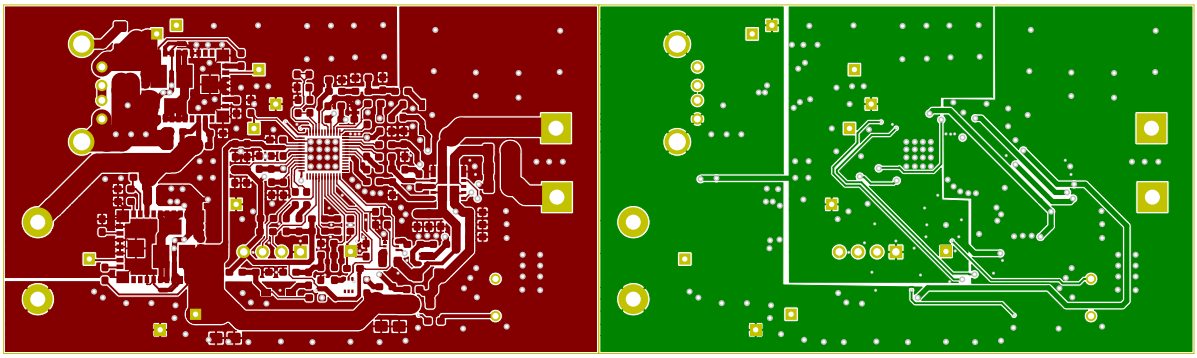

(a) Front copper layer of the PCB. (b) Back copper layer of the PCB

Figure 7.1: Copper layers of the PCB.

7.2. Complete system

A 3D render of the Powerlizer including its subsystems can be seen in Figure 7.2. A phone can be seen next to it for scale. The UV-C disinfection LEDs are integrated into the lid that can open and close. The batteries are located in the closed-off part in the front. The bottom layer where the phone can lie has been made transparent to reveal the PCBs and shielding underneath. This part of the prototype was not fabricated.

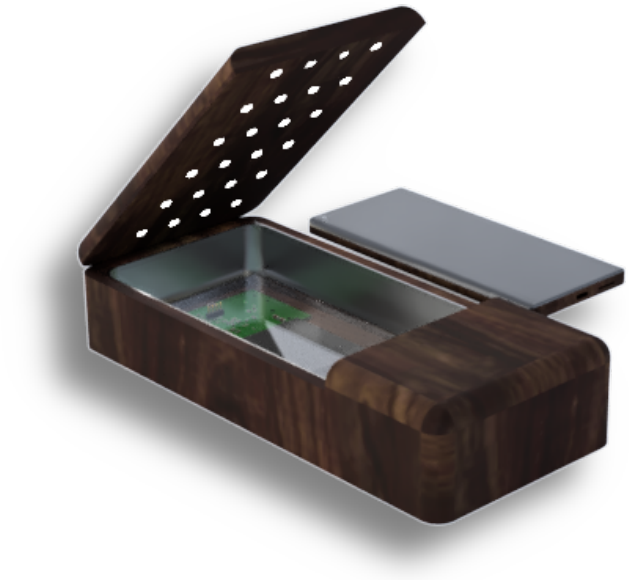

Figure 7.2: 3D render of the Powerlizer.

7.3. Testing

After the wireless charging system PCB was assembled several measurements were done to test the functionality of the prototype. First, the buck converter's performance was tested. Then, correct behaviour of the full-bridge inverter was indicated on the transmitting coil and the power transfer efficiency was measured at 5 W.

The 12 V buck converter was tested by connecting a 6 Ω resistor to the output. This creates the

same load condition as applied in the component's simulation in section 5.1.6. Figure 7.3 compares the buck converter's output voltage during startup in orange with the corresponding LTspice simulation in blue. The figure shows that the prototype's buck converter takes approximately 3 ms longer to reach the required output of (12 ± 1) V. This will not have a important effect the performance to the wireless charger. More importantly the buck converter reaches and maintains 11.92 V on its output. The efficiency of the buck converter attached to a 6 Ω load was 84 %.

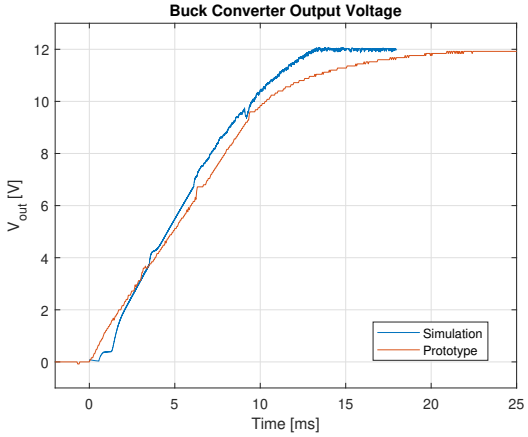

Figure 7.3: Buck converter output voltage during startup.

Figure 7.4 shows the voltage measured across the transmitter coil during the Ping phase. From it, it can be concluded that the inverter can correctly invert the 12 V DC voltage into a 24 V peak-to-peak AC signal and can do it at 143 kHz, the high end of the required frequency range of 110–145 kHz.

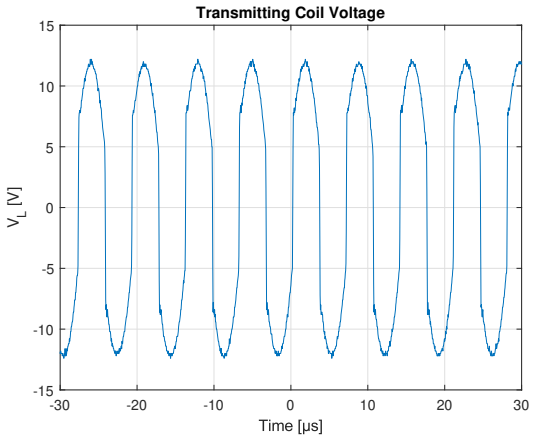

Figure 7.4: Coil voltage during operation of full-bridge inverter

To test the efficiency of the system, the PCB was connected to a power supply and the input- and output power were measured. The output of the receiver was connected to a 5.0 Ω resistor and the power supply was set to 15 V. With these settings, the input current was measured to be 0.44 A and the output voltage of the receiver was measured to be 4.7 V. The efficiency was calculated using Equation 7.1. This measurement was done using a 5 W Qi receiver. The efficiency at 15 W was not measured as no receiver was available but this efficiency is expected to be higher. This is also indicated in the datasheet of the Qi IC [25].

$$\eta = \frac{P_{out}}{P_{in}} = \frac{(\frac{V_{out}^2}{R_{out}})}{I_{in}V_{in}} = 67\,\% \tag{7.1}$$

8

Conclusion

This thesis presented the design of a wireless charging system that can be implemented in a power bank that performs wireless phone charging and sterilization with UV-C light, the Wireless Powerlizer. The focus in wireless charging system design was put on the power management in transferring 15 to 21 V DC battery power to the receiving coil of a wireless charging phone. This entailed the design of a buck converter, a full-bridge inverter, and a series compensated wireless charging coil.

The buck converter was designed to be implemented with an IC of which the required operation was achieved through the selection of external components. Output voltage ripple was calculated through circuit analysis and the output voltage, output current, startup behavior, and voltage ripple were verified through LTspice simulation.

The full-bridge inverter was designed by setting up requirements for the MOSFETs and power dissipation was tested through LTspice simulation with the selected MOSFETs. The control of the inverter to manage the power transfer and communication with the charging phone was implemented with an off-the-shelf Qi standard communication IC.

A prototype of this design was also assembled and tested. These tests revealed the prototype's ability to transfer 5 W of power wirelessly to the power receiver of a phone. This was also achieved with an efficiency of 67 % well above the 50 % requirement [**M.3**]. This is the most important metric for the battery powered charger and therefore indicates a successful design. At higher power transfer the efficiency is expected to be higher, as simulations showed 74 % efficiency at 15 W.

The system was also designed to adhere to all the other requirements set in Chapter 2. The adherence to these requirements was verified by simulation as much as possible. The foreign object detection, temperature and safety requirements [**M.5**], [**M.7**] and [**S.1**] could not be properly verified before a functioning prototype was realised, after which time constraints and logistical problems obstructed these tests.

To conclude, a full wireless charging system was designed that successfully adhered to all requirements that could be tested and a prototype was built and used to indicate correct behavior and adherence to the imporant efficiency requirement. However, limited time with the working prototype caused insufficient or no verification of certain requirements.

8.1. Recommendations

Although this thesis presents a full design for a wireless charging system there is still much to be done to ensure the required performance for implementation in the Wireless Powerlizer. This section presents some recommendations for the future development of the wireless charging system.

FOD and thermal testing

Although a working prototype was realised by the end of this project, there was not enough time to perform the FOD and thermal testing that was planned. It is therefore important that these aspects of the prototype are verified. A new prototype should be build according to the version 2 schematic in Appendix B.3, where some errors in the current prototype are fixed. It would also be useful to integrate the next prototype with the other parts of the Powerlizer.

EMI Testing
Testing on the system's ability to interfere with an external device through electromagnetic inference is necessary to ensure the adherence to requirement [**S.1**]. Simulations in Section 6.1.2 show that the magnetic field strength stayed within legal limits. Further real-world testing did not fall within the scope of this thesis.

Updating to the Latest Qi Standard
Access to the latest version of the Qi standard involved substantial fees. Therefore, the system design in this thesis follows Qi standard version 1.2.3 from 2017. Adherence to the latest version of the Qi standard is unlikely to require a lot of redesign, but it is something to look into once this is possible.

A

Abbreviations

A.1. List of Abbreviations

Abbreviation	Description
AC	Alternating Current
ASK	Amplitude Shift Keying
AWG	American Wire Gauge
BOM	Bill Of Materials
CISPR	Comité International Spécial des Perturbations Radioélectriques
DC	Direct Current
EMC	ElectroMagnetic Compatibility
EMI	ElectroMagnetic Interference
FOD	Foreign Object Detection
FSK	Frequency Shift Keying
IC	Integrated Circuit
IEC	International Electrotechnical Commission
ISO	International Organisation for Standardisation
laser	Light Amplification by Stimulated Emission of Radiation
LED	Light Emitting Diode
LTspice	Linear Technology Simulation Program with Integrated Circuit Emphasis
MOSFET	Metal-Oxide-Semiconductor Field-Effect Transistor
MP	Medium Power
PCB	Printed Circuit Board
PID	Proportional–Integral–Derivative controller
RX	Receiver
SEPIC	Single-ended primary-inductor converter
TX	Transmitter
USB	Universal Serial Bus
WPC	Wireless Power Consortium
WPT	Wireless Power Transfer

B

Appendix

B.1. Buck Converter Circuit

```
XU1 N002 N002 N003 N004 N002 NC_01 out 0 NC_02 0 NC_03 NC_04 0 0 NC_05
    NC_06 0 0 out out out out out out 0 0 0 0 0 NC_07 NC_08 NC_09 NC_10
    NC_11 N001 N005 N006 0 0 N007 0 TPS84250_TRANS
R1 N001 N005 174k
R2 N005 0 16k
R3 0 N007 267k
R5 N004 out 140k
V1 N001 0 15 Rser=1m
C2 N006 0 22n Rser=10m
C3 out 0 47µ Rser=10m
C4 out 0 47µ Rser=10m
C1 N001 0 4.4µ Rser=10m
R4 out 0 6
R6 N001 N003 100k
.tran 1 uic
* Setting the \nOutput voltage
* Under-voltage Lockout
* Setting the \nSwitching Frequency
* Slow Start
* Buck Converter IC
.lib C:\Users\Floris\Downloads\tps84250.lib
.backanno
.end
```

B.2. Equivalent Circuit

```
L_TX N006 FB2 10µ Rser=50m
L_RX N009 N007 44.8µ Rser=1
C_c N006 FB1 247n Rser=2m
C2 N008 N007 56n Rser=2m
C3 N009 N008 0.8n Rser=2m
C4 N005 0 33µ
D1 N008 N005 MURS320
D2 N009 N005 MURS320
D3 0 N009 MURS320
D4 0 N008 MURS320
XU3 FB1 G3 0 DMHT3006LFJ
```

```
XU2 12V G2 FB2 DMHT3006LFJ
XU4 FB2 G4 0 DMHT3006LFJ
V1 N001 FB1 PULSE(0 5 0.7e-6 150e-9 150e-9 3.2e-6 8e-6)
V3 N003 0 PULSE(5 0 0.1e-6 50e-9 50e-9 4.8e-6 8e-6)
V5 12V 0 12 Rser=100m
C5 12V 0 47µ Rser=2m
C6 12V 0 47µ Rser=2m
R1 G1 N001 12
R4 G4 N004 12
XU1 12V G1 FB1 DMHT3006LFJ
V4 N004 0 PULSE(0 5 0.8e-6 50e-9 50e-9 3.2e-6 8e-6)
V2 N002 FB2 PULSE(5 0 0 150e-9 150e-9 4.8e-6 8e-6)
R2 G2 N002 12
R3 G3 N003 12
V6 N005 0 12 Rser=100m
.model D D
.lib C:\Users\brech\Documents\LTspiceXVII\lib\cmp\standard.dio
k L_TX L_RX 0.63
.tran 0.5ms
* Input supply
* Gate drivers
* Full-bridge inverter
* Magnetic resonant circuit
* Output supply
.lib C:\Users\brech\Downloads\DMHT3006LFJ.spice.txt
.backanno
.end
```

B.3. PCB

The PCB was designed according to the the version one schematic as seen below. Several errors were corrected in version two of the schematic seen below the version one schematic. The connections of R34, R35, IC4 and IC5 have changed. Extra connections were also added to SW_BRG1 and SW_BRG2 of IC1. The input of the voltage sense and communication demodulation circuit were also connected to the correct side of the compensation.

Qi chip

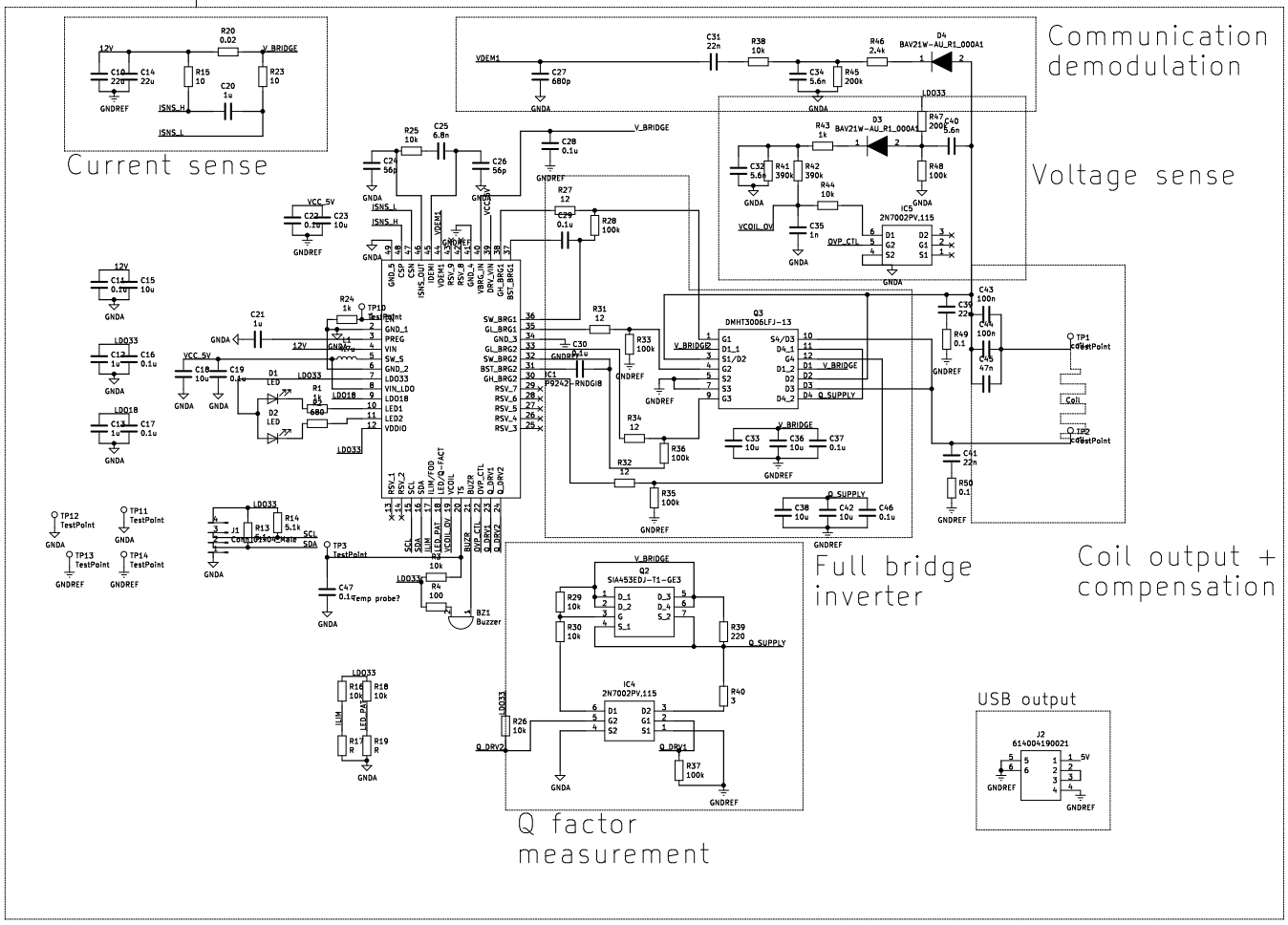

12V Regulator

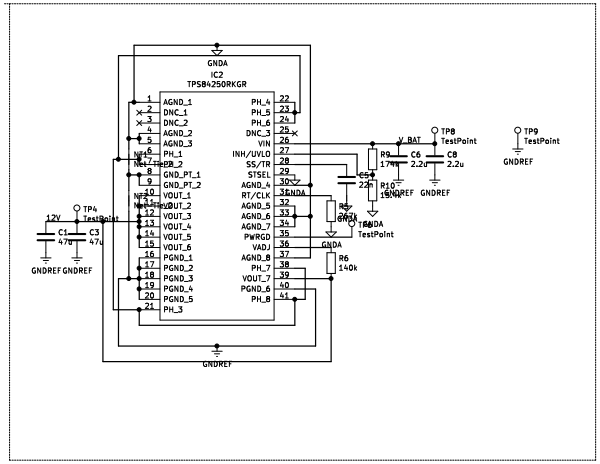

5V Regulator

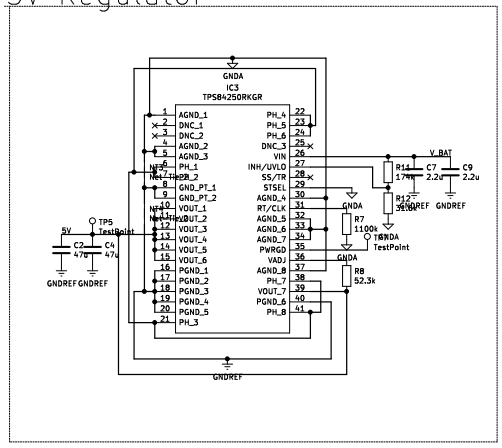

Sheet: /	
File: BAP.sch	
Title: Version 1 Schematic	
Size: User	Date:
KiCad E.D.A. eeschema (5.1.4)-1	Rev: 1
	Id: 1/1

Qi chip

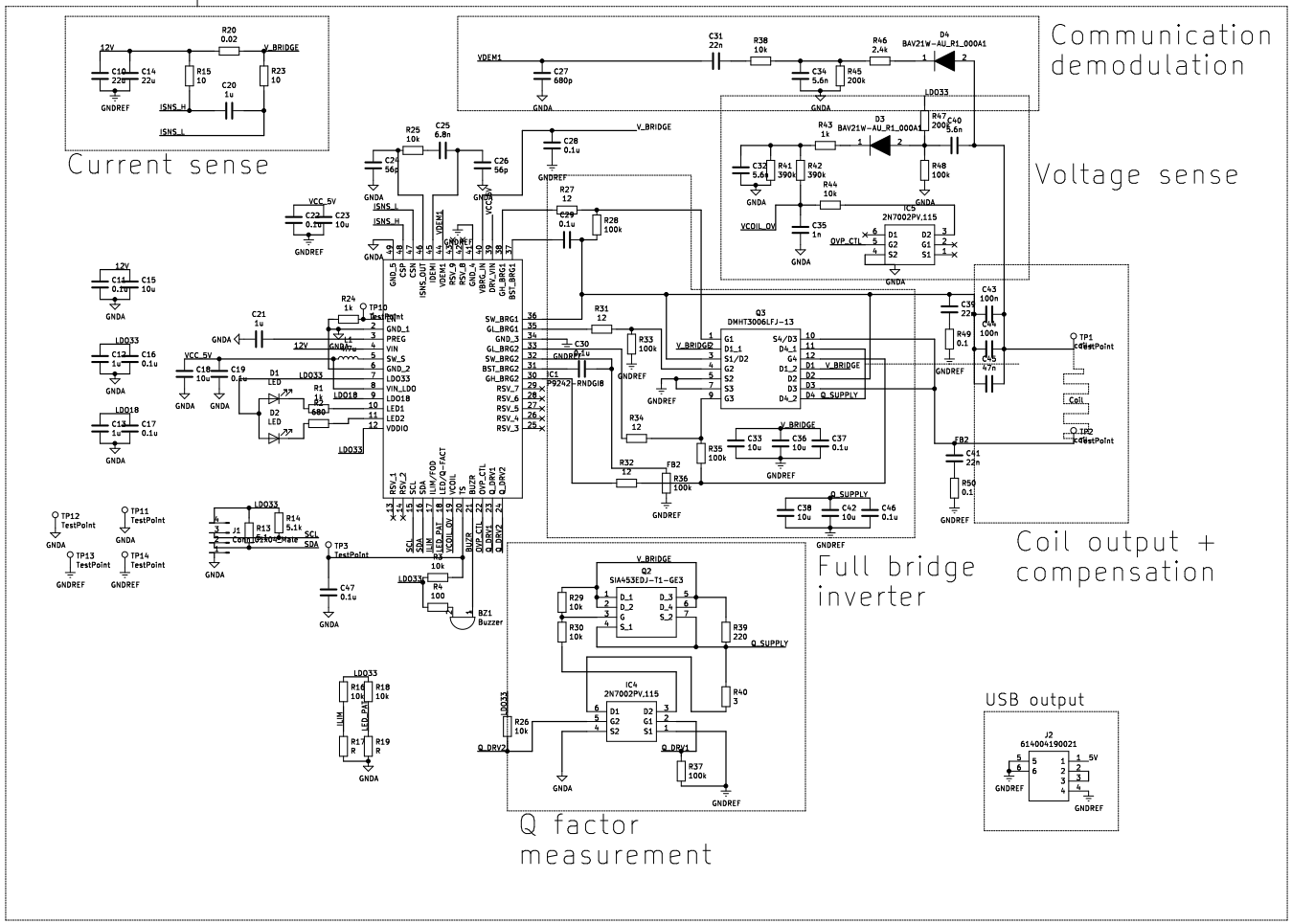

12V Regulator

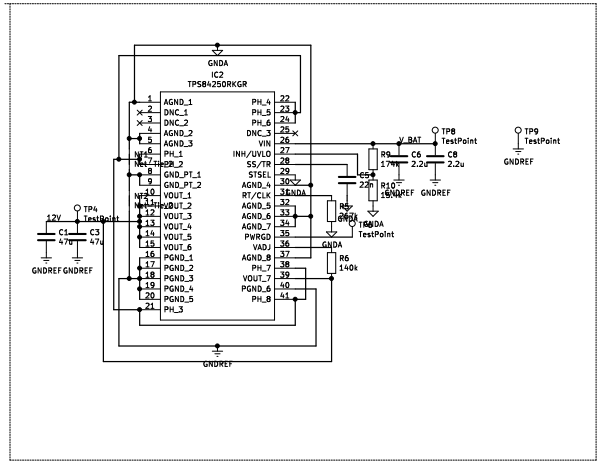

5V Regulator

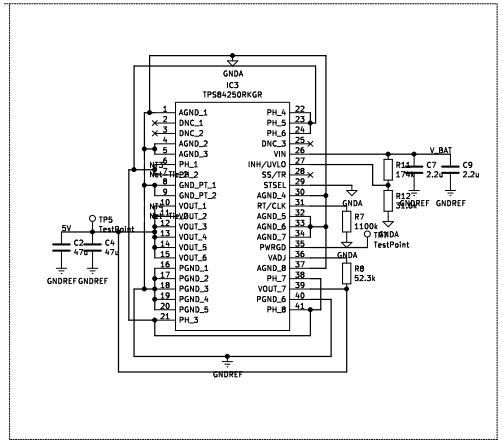

Sheet: /	
File: BAPv2.sch	
Title: Version 2 Schematic	
Size: User	Date:
KiCad E.D.A. eeschema (5.1.4)-1	Rev: 2
	Id: 1/1

Table B.1: Bill of material list.

Mouser Number	Manufacturer Number	Manufacturer	Description	Quantity
80-C0603C104K3R	C0603C104K3RACTU	KEMET	Multilayer Ceramic Capacitors MLCC - SMD/SMT 25V 0.1uF X7R 0603 10%	12
81-GRM188R61E106KA3D	GRM188R61E106KA73D	Murata	Multilayer Ceramic Capacitors MLCC - SMD/SMT 10UF 25V 10% 0603	7
810-CGB3B1X5R1E105MC	CGB3B1X5R1E105M055AC	TDK	Multilayer Ceramic Capacitors MLCC - SMD/SMT RECOMMENDED ALT 810-CGB3B1X5R1E105KC	4
581-06035A560JAT4A	06035A560JAT4A	AVX	Multilayer Ceramic Capacitors MLCC - SMD/SMT 50V 56pF C0G 0603 5%	2
710-885012206040	885012206040	Wurth Elektronik	Multilayer Ceramic Capacitors MLCC - SMD/SMT WCAP-CSGP 0.01uF 0603 10% 16V MLCC	1
581-06035C223K4	06035C223K4T2A	AVX	Multilayer Ceramic Capacitors MLCC - SMD/SMT 50V 0.022uF X7R 0603 10% AEC-Q200	2
80-C0603C681K5R	C0603C681K5RACTU	KEMET	Multilayer Ceramic Capacitors MLCC - SMD/SMT 50V 680pF X7R 0603 10%	1
581-06035C102KAT4A	06035C102KAT4A	AVX	Multilayer Ceramic Capacitors MLCC - SMD/SMT 50V 1000pF X7R 0603 10%	1
810-C1608C0G2A562J8C	C1608C0G2A562J080AC	TDK	Multilayer Ceramic Capacitors MLCC - SMD/SMT 0603 100V 5600pF C0G 5% T: 0.8mm	3
810-C3216C0G2A104J6C	C3216C0G2A104J160AC	TDK	Multilayer Ceramic Capacitors MLCC - SMD/SMT 1206 100V 0.1uF C0G 5% T: 1.6mm	2
81-GRM155R71H223KA2J	GRM155R71H223KA12J	Murata	Multilayer Ceramic Capacitors MLCC - SMD/SMT 0.022uF 50Volts X7R 10%	1
810-C3216C0G2A683J6C	C3216C0G2A683J160AC	TDK	Multilayer Ceramic Capacitors MLCC - SMD/SMT 1206 100V 0.068uF C0G 5% T: 1.6mm	1
810-C3216C0G2A473JAC	C3216C0G2A473J115AC	TDK	Multilayer Ceramic Capacitors MLCC - SMD/SMT 1206 100V 0.047uF C0G 5% T: 1.15mm	1
581-12063D226KAT2A	12063D226KAT2A	AVX	Multilayer Ceramic Capacitors MLCC - SMD/SMT 25V 22uF X5R 1206 10%	2
581-06035C104KAT2A	06035C104KAT2A	AVX	Multilayer Ceramic Capacitors MLCC - SMD/SMT 50V 0.1uF X7R 0603 10%	1
81-GRM188R61E475KE5D	GRM188R61E475KE15D	Murata	Multilayer Ceramic Capacitors MLCC - SMD/SMT 4.7UF 25V 10% 0603	1
710-150060RS75000	150060RS75000	Wurth Elektronik	Standard LEDs - SMD WL-SMCW SMDMono TpVw Waterclr 0603 Red	1
710-150060GS75000	150060GS75000	Wurth Elektronik	Standard LEDs - SMD WL-SMCW SMDMono TpVw Waterclr 0603 Green	1
81-LQM18PN4R7MFRL	LQM18PN4R7MFRL	Murata	Fixed Inductors 0603 4.7uH 20%	1
810-PS1240P02CT3	PS1240P02CT3	TDK	Piezo Buzzers & Audio Indicators Round 12.2mmx3.5mm 4kHz Vin=3V	1
594-NTCLE203E3103JB0	NTCLE203E3103JB0	Vishay	NTC (Negative Temperature Coefficient) Thermistors 10Kohms 5% Radial	1
603-RC0603DR-071KL	RC0603DR-071KL	Yageo	Thick Film Resistors - SMD 1 kOhms 100 mW 0603 1%	3
755-SFR03EZPF6800	SFR03EZPF6800	ROHM Semiconductor	Thick Film Resistors - SMD 0603 680ohm 1% Anti-Sulfur AEC-Q200	1
755-SFR03EZPF1002	SFR03EZPF1002	ROHM Semiconductor	Thick Film Resistors - SMD 0603 10Kohms 1% Anti-Sulfur AEC-Q200	9
667-ERJ-S03F1003V	ERJ-S03F1003V	Panasonic	Thick Film Resistors - SMD 0603 100Kohms 1% Anti-Sulfur	5
603-RC0603JR-07100RL	RC0603JR-07100RL	Yageo	Thick Film Resistors - SMD 100 Ohms 100 mW 0603 5%	1
667-ERJ-3GEYJ394V	ERJ-3GEYJ394V	Panasonic	Thick Film Resistors - SMD 0603 390Kohms 5% AEC-Q200	2
667-ERJ-PA3D2401V	ERJ-PA3D2401V	Panasonic	Thick Film Resistors - SMD 0603 2.4Kohm 0.5% Anti-Surge AEC-Q200	1
667-ERJ-3EKF2003V	ERJ-3EKF2003V	Panasonic	Thick Film Resistors - SMD 0603 200Kohms 1% AEC-Q200	2
71-CRCW060310R0FKEAC	CRCW060310R0FKEAC	Vishay	Thick Film Resistors - SMD 1/10Watt 10ohms 1% Commercial Use	2
71-WSL0805R0200FEA	WSL0805R0200FEA	Vishay	Current Sense Resistors - SMD 1/8watt .02ohms 1%	1
71-CRCW0603-12-E3	CRCW060312R0FKEA	Vishay	Thick Film Resistors - SMD 1/10watt 12ohms 1%	4
71-CRCW08053R00FNEA	CRCW08053R00FNEA	Vishay	Thick Film Resistors - SMD 1/8watt 3ohms 1% 200ppm	1
71-CRCW0603100KFKEAC	CRCW0603100KFKEAC	Vishay	Thick Film Resistors - SMD 1/10Watt 100Kohms 1% Commercial Use	1
667-ERJ-L03KF10CV	ERJ-L03KF10CV	Panasonic	Current Sense Resistors - SMD 0603 0.1ohm 1% Curr Sense AEC-Q200	1
755-ESR10EZPF2200	ESR10EZPF2200	ROHM Semiconductor	Thick Film Resistors - SMD 0805 220ohm 1% Anti Surge AEC-Q200	2
81-GRM188R61E225MA2D	GRM188R61E225MA12D	Murata	Multilayer Ceramic Capacitors MLCC - SMD/SMT 0603 2.2uF 25volts X5R 20%	4
80-C0603C223J3R	C0603C223J3RACTU	KEMET	Multilayer Ceramic Capacitors MLCC - SMD/SMT 25V 0.022uF X7R 0603 5%	1
754-RR0816P-1743D24D	RR0816P-1743-D-24D	Susumu	Thin Film Resistors - SMD 1/16W 174Kohm 0.5% 25ppm	2
754-RR0816P-163D	RR0816P-163-D	Susumu	Thin Film Resistors - SMD 1/16W 16Kohm 0.5% 25ppm	1
667-ERJ-3EKF2673V	ERJ-3EKF2673V	Panasonic	Thick Film Resistors - SMD 0603 267Kohms 1% AEC-Q200	1
754-RR0816P-1403D15D	RR0816P-1403-D-15D	Susumu	Thin Film Resistors - SMD 1/16W 140Kohm 0.5% 25ppm	1
754-RR0816P-3162D49C	RR0816P-3162-D-49C	Susumu	Thin Film Resistors - SMD 1/16W 31.6Kohm 0.5% 25ppm	1
71-CRCW06031M10FKEA	CRCW06031M10FKEA	Vishay	Thick Film Resistors - SMD 1/10watt 1.1Mohms 1%	1
754-RR0816P-5232D70C	RR0816P-5232-D-70C	Susumu	Thin Film Resistors - SMD 1/16W 52.3Kohm 0.5% 25ppm	1
810-C3216X5R1E476M	C3216X5R1E476M160AC	TDK	Multilayer Ceramic Capacitors MLCC - SMD/SMT 1206 25VDC 47uF 20% X5R 1.6mm	4
972-P9242-RNDGI8	P9242-RNDGI8	Renesas Electronics	Wireless Charging ICs WPC 1.2.2 Wireless Transmitter 15W	1
810-WT52522512F2MA2G	WT525225-12F2-MA2-G	TDK	Wireless Charging Coils Tx Wireless Charging Coil 10.5uH 0.06ohm	1
595-TPS84250RKGR	TPS84250RKGR	Texas Instruments	Switching Voltage Regulators 7V-50Vin,2.5A SD Integrated Power Sol	2
621-DMHT3006LFJ-13	DMHT3006LFJ-13	Diodes Incorporated	MOSFET MOSFET BVDSS: 25V-30V	1
710-614004190021	614004190021	Wurth Elektronik	USB Connectors WR-COM USB Type A THT Horizontal	1
78-SIA453EDJ-T1-GE3	SIA453EDJ-T1-GE3	Vishay	MOSFET RECOMMENDED ALT 78-SIA441DJ-T1-GE3	1
771-2N7002PV-115	2N7002PV,115	Nexperia	MOSFET MOSFET N-CH DUAL 60V	2
241-BAV21W-AUR1000A1	BAV21W-AU_R1_000A1	Panjit	Diodes - General Purpose, Power, Switching /A82/TR/7"/HF/3K/SOD-123/SWI/SOD/USM-04/USM04-QI04/PJ///	2
187-CL10A105KA8NFNC	CL10A105KA8NFNC	Samsung Electro-Mechanics	Multilayer Ceramic Capacitors MLCC - SMD/SMT 1uF+/-10% 25V X5R 1608	1
660-SG73G2BTTD2200D	SG73G2BTTD2200D	KOA Speer	Thick Film Resistors - SMD 220 ohm 0.5% 0.5W AEC-Q200	1

B.4. Derivations

B.4.1. Capacitor Charge Fluctuation

A linear increase in inductor current when the buck converter MOSFET is closed and the linear decrease when the MOSFET is open leads to an inductor and capacitor current ripple as shown in figure B.1, based on equation 5.6.

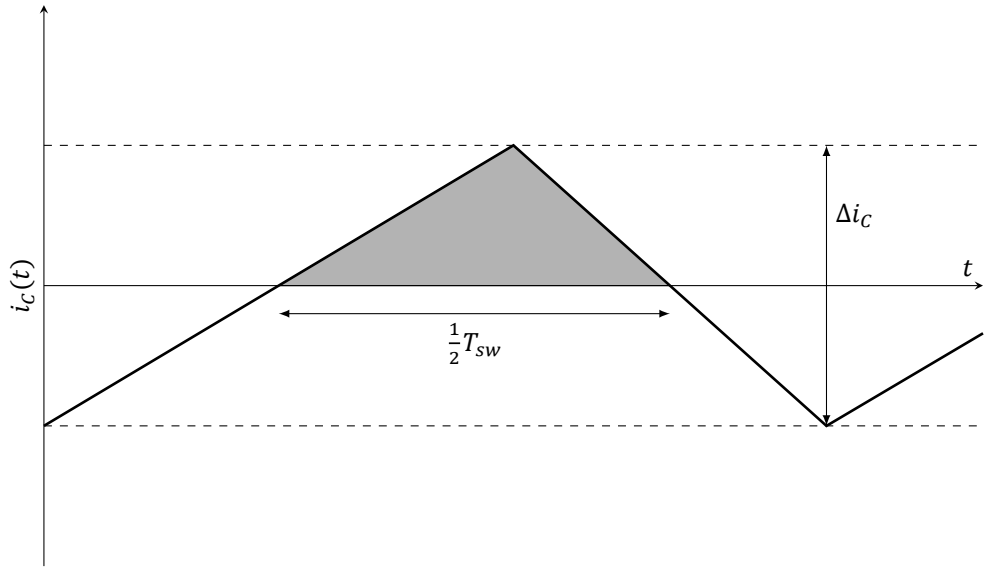

Figure B.1: Capacitor current

The charge fluctuation in the capacitor is then equal to the integration of the above average current $i_L(t) - I_L$ as shown by the grey area in figure B.1. This integration is performed over half the switching period of the converter as in equation B.1.

$$\Delta Q = \int_{t}^{t+\frac{1}{2}T_{sw}} (i_L(t) - I_L)\, dt \tag{B.1}$$

In this integral $(i_L(t) - I_L)$ has an average value of one quarter of Δi_L, so equation B.1 becomes equation B.2.

$$\Delta Q = \frac{1}{4}\Delta i_L * \frac{1}{2}T_{sw} = \frac{1}{8}\frac{\Delta i_L}{f_{sw}} \tag{B.2}$$

B.4.2. Electrical circuit

Using Kirchhoff's voltage- and current law, the following equations were obtained:

$$V_{in} - I_1 Z_{C_c} - I_1 Z_{TX} - j\omega M I_2 = 0 \tag{B.3}$$

$$-Z_{RX} - j\omega M I_1 - Z_{C_1} I_2 = V_{out} \tag{B.4}$$

$$I_4 = \frac{-V_{out}}{Z_{C_2}} \tag{B.5}$$

$$I_3 = I_2 - I_4 \tag{B.6}$$

Rewriting these equations gives:

$$I_1 = \frac{V_{in}(Z_{C_1} + Z_{RX}) + j\omega M V_{out}}{M^2\omega^2 + (Z_{C_1} + Z_{RX})(Z_{C_c} + Z_{TX})} \tag{B.7}$$

$$I_3 = \frac{V_{out}}{Z_{C_2}} - \frac{V_{out}}{Z_{C_1} + Z_{RX}} - \frac{j\omega M(V_{in}(Z_{C_1} + Z_{RX}) + j\omega M V_{out})}{(Z_{C_1} + Z_{RX})(M^2\omega^2 + (Z_{C_1} + Z_{RX})(Z_{C_c} + Z_{TX}))} \tag{B.8}$$

Using these equations, the input impedance and the efficiency can be calculated:

$$Z_{in} = \frac{V_{in}}{I_1} = \frac{V_{in}(M^2\omega^2 + (Z_{C_1} + Z_{RX})(Z_{C_c} + Z_{TX}))}{V_{in}(Z_{C_1} + Z_{RX}) + j\omega M V_{out}} \tag{B.9}$$

$$\eta = \frac{-I_3 V_{out}}{I_1 V_{in}} = \tag{B.10}$$

$$\frac{-V_{out}(V_{out}M^2\omega^2 - jM\omega V_{in}Z_{C_2} + V_{out}Z_{C_1}Z_{C_c} - V_{out}Z_{C_2}Z_{C_c} + V_{out}Z_{C_c}Z_{RX} + V_{out}Z_{C_1}Z_{TX} - V_{out}Z_{C_2}Z_{TX} + V_{out}Z_{RX}Z_{TX})}{V_{in}Z_{C_2}(V_{in}Z_{C_1} + V_{in}Z_{RX} + j\omega M V_{out})} \tag{B.11}$$

Bibliography

[1] Jeroen van Ammers and Hsukang Chen. Battery Management System for the Wireless Powerlizer, 2021. URL http://resolver.tudelft.nl/uuid:619b98e6-4710-484d-bf52-60ccadf5be7e. Bachelor Thesis, Delft University of Technology.

[2] Charlotte De Jonghe and Gijs Lageweij. UV-C Sterilizer for the Wireless Powerlizer, 2021. URL http://resolver.tudelft.nl/uuid:6d850912-a034-4f34-8de1-283041ffb852. Bachelor Thesis, Delft University of Technology.

[3] Viktor Shevchenko, Oleksandr Husev, Ryszard Strzelecki, Bohdan Pakhaliuk, Nikolai Poliakov, and Natalia Strzelecka. Compensation Topologies in IPT Systems: Standards, Requirements, Classification, Analysis, Comparison and Application. *IEEE Access*, 7:120559–120580, 2019. doi:10.1109/ACCESS.2019.2937891.

[4] Chenggang Fang, Jiancheng Song, Lingyan Lin, and Yameng Wang. Practical considerations of series-series and series-parallel compensation topologies in wireless power transfer system application. In *2017 IEEE PELS Workshop on Emerging Technologies: Wireless Power Transfer (WoW)*, pages 255–259, 2017. doi:10.1109/WoW.2017.7959404.

[5] Yijie Wang, Yousu Yao, Xiaosheng Liu, Dianguo Xu, and Liang Cai. An LC/S Compensation Topology and Coil Design Technique for Wireless Power Transfer. *IEEE Transactions on Power Electronics*, 33(3):2007–2025, 2018. doi:10.1109/TPEL.2017.2698002.

[6] Yiming Zhang, Tianze Kan, Zhengchao Yan, Yunhe Mao, Zhixian Wu, and Chunting Chris Mi. Modeling and Analysis of Series-None Compensation for Wireless Power Transfer Systems With a Strong Coupling. *IEEE Transactions on Power Electronics*, 34(2):1209–1215, 2019. doi:10.1109/TPEL.2018.2835307.

[7] URL https://www.pcna.com/en-ca/product/ultra-thin-fabric-wireless-charging-pad-7141-83

[8] URL https://www.amazon.nl/Standaard-Ontvangermodule-Spoelontvangermodule-Printplaat-be dp/B08CB7FPHF/.

[9] The Qi Wireless Power Transfer System Power Class 0 Specification. Technical report, Wireless Power Consortium, 2017. URL https://www.wirelesspowerconsortium.com/knowledge-base/specifications/download-the-qi-specifications.html.

[10] Qingwen Liu, Jun Wu, Pengfei Xia, Shengjie Zhao, Wei Chen, Yanping Yang, and Lajos Hanzo. Charging Unplugged: Will Distributed Laser Charging for Mobile Wireless Power Transfer Work? *IEEE Vehicular Technology Magazine*, 11(4):36–45, 2016. doi:10.1109/MVT.2016.2594944.

[11] S. Y. Hui. Planar Wireless Charging Technology for Portable Electronic Products and Qi. *Proceedings of the IEEE*, 101(6):1290–1301, 2013. doi:10.1109/JPROC.2013.2246531.

[12] Kaspars Kroičs and Janis Voitkans. High frequency two-plate capacitive wireless power transfer system. 05 2018. doi:10.22616/ERDev2018.17.N432.

[13] Koenraad Van Schuylenbergh and Robert Puers. *Inductive Powering Basic Theory and Application to Biomedical Systems*. Springer, Leuven, Belgium, 2009.

[14] James C. Lin. Wireless Power Transfer for Mobile Applications, and Health Effects [Telecommunications Health and Safety]. *IEEE Antennas and Propagation Magazine*, 55(2):250–253, 2013. doi:10.1109/MAP.2013.6529362.

[15] Byung-Jun Jang, Seongjoo Lee, and Hyungoo Yoon. HF-Band Wireless Power Transfer System: Concept, Issues, and Design. *Progress In Electromagnetics Research*, 124:211–231, January 2012. doi:10.2528/PIER11120511.

[16] Jia Hou, Qianhong Chen, Kaiqin Yan, Xiaoyong Ren, Siu-Chung Wong, and Chi. K Tse. Analysis and control of S/SP compensation contactless resonant converter with constant voltage gain. In *2013 IEEE Energy Conversion Congress and Exposition*, pages 2552–2558, 2013. doi:10.1109/ECCE.2013.6647030.

[17] M. Galizzi, M. Caldara, V. Re, and A. Vitali. A novel Qi-standard compliant full-bridge wireless power charger for low power devices. In *2013 IEEE Wireless Power Transfer (WPT)*, pages 44–47, 2013. doi:10.1109/WPT.2013.6556877.

[18] Alexander Bubovich. The comparison of different types of DC-DC converters in terms of low-voltage implementation. In *2017 5th IEEE Workshop on Advances in Information, Electronic and Electrical Engineering (AIEEE)*, pages 1–4, 2017. doi:10.1109/AIEEE.2017.8270560.

[19] Robert W. Ericson and Dragan Maksimović. *Fundamentals of Power Electronics*. Springer International Publishing, 3 edition, 2020. ISBN 978-3-030-43881-4. doi:10.1007/978-3-030-43881-4.

[20] Robert Keim. How to Choose the Frequency of Your Switching Regulator. *All About Circuits*, June 2018. URL https://www.allaboutcircuits.com/technical-articles/how-to-choose-the-frequency-of-your-switching-regulator/.

[21] Terry Remple and Adam Burns. Battery Charging Specification Revision 1.2. Technical report, USB, December 2017. URL https://usb.org/document-library/battery-charging-v12-spec-and-adopters-agreement.

[22] Trace Engineering. A Review of Inverter Design and Topologies. URL http://www.dieselduck.info/machine/04%20auxiliary/2000%20Inverter%20technology.pdf. Rev 2/00.

[23] W. P. Choi, W. C. Ho, X. Liu, and S. Y. R. Hui. Comparative study on power conversion methods for wireless battery charging platform. In *Proceedings of 14th International Power Electronics and Motion Control Conference EPE-PEMC 2010*, pages S15–9–S15–16, 2010. doi:10.1109/EPEPEMC.2010.5606675.

[24] George Lakkas. MOSFET power losses and how they affect power-supply efficiency. Technical report, Texas Instruments, 2016. URL https://www.ti.com/lit/an/slyt664/slyt664.pdf?ts=1623609284285&ref_url=https%253A%252F%252F.

[25] Renesas Electronics Corporation. P9242-R Datasheet, March 2020. URL https://www.renesas.com/us/en/document/dst/p9242-r-datasheet?language=en&r=192036. Revision 1.0.

[26] Zeljko Pantic and Srdjan Lukic. Computationally-Efficient, Generalized Expressions for the Proximity-Effect in Multi-Layer, Multi-Turn Tubular Coils for Wireless Power Transfer Systems. *IEEE Transactions on Magnetics*, 49(11):5404–5416, 2013. doi:10.1109/TMAG.2013.2264486.

[27] Minister van Economische Zaken. Regeling gebruik van frequentieruimte zonder vergunning en zonder meldingsplicht 2015, 2015. https://wetten.overheid.nl/BWBR0036378/2016-12-28.

[28] Diodes Incorporated. DMHT3006LFJ SPICE Model, May 2016. URL https://www.diodes.com/spice/download/3979/DMHT3006LFJ.spice.txt. Version 1.0M.

[29] Texas Instruments. TPS84250 Datasheet, April 2018. URL https://www.ti.com/lit/ds/symlink/tps84250.pdf. Revision C.